RSC Advances

REVIEW

View Article Online
View Journal | View Issue

Cite this: *RSC Adv.*, 2026, **16**, 6706

Saussurea costus in nanomedicine: green-synthesized metal nanoparticles and advanced nanosystems for enhanced therapeutic efficacy

Jude Majed Lababidi and Hassan Mohamed El-Said Azzazy *

Saussurea costus (*S. costus*), a medicinal plant widely utilized in traditional Ayurveda, Chinese, and Tibetan medicine, is rich in pharmacologically active compounds, including sesquiterpene lactones, flavonoids, phenolics, and essential oils. Despite its reported antimicrobial, anti-inflammatory, antioxidant, anticancer, and immunomodulatory activities, clinical translation of *S. costus* remains hindered by its low bioavailability and off-target effects. This review explores the use of nanosystems to address these limitations and enhance the biological performance of *S. costus* extracts. Metal-based nanoparticles (silver, copper, palladium, magnesium oxide) and other nano-formulations, including polymeric, lipid-based, and inorganic nanoparticles, detailing their synthesis, characterization techniques, and biomedical applications. The integration of *S. costus* into nanosystems is shown to improve cellular uptake and facilitate prolonged release and superior therapeutic outcomes as supported by several *in vitro* and *in vivo* studies. This review highlights the incorporation of *Saussurea costus* into different nanosystems towards the development of effective nanotherapeutics.

Received 21st November 2025
Accepted 2nd January 2026

DOI: 10.1039/d5ra09018k

rsc.li/rsc-advances

1. Introduction

The genus *Saussurea*, a member of the Asteraceae family, comprises over 400 species globally.[1,2] These are widely distributed across temperate regions, such as south and central Asia, China, Himalayas, and Russia.[3,4] *Saussurea* species growing in alpine and subalpine regions has diverse phytochemicals as a mechanism for adaptation and survival in such unique environments.[5] The botanical diversity of this plant, as well as the various morphologically distinct members ranging from low-growing herbs to taller perennial species, reflect the wide spectrum of pharmacological applications across different species.[6] Several *Saussurea* species, including *Saussurea costus* (synonym: *S. lappa*), *S. laniceps*, *S. obvallata*, *S. involucrate*, and *S. gossypiphora* are traditionally used in different medicine systems such as Traditional Chinese Medicine (TCM), Ayurveda, Tibetan, and Korean medicine.[1,7–10] These species have been utilized in the treatment of various illnesses such as digestive disorders,[11] respiratory diseases,[12,13] inflammatory conditions,[10,14] gynecological issues,[15] and infectious diseases.[16] Among the genus, *Saussurea costus* (*S. costus*), known for its significant use in various traditional medicine in Pakistan and Himalayan region of India. For instance, In Ayurvedic medicine, *S. costus* was utilized to treat asthma, inflammatory diseases, ulcers, and stomach disorders.[17] Within the Unani system, the root of *S. costus* is used to treat kidney, liver, and blood diseases. It is also known to be employed as a carminative, anthelmintic, and brain stimulant.[18]

The phytochemical analyses of *S. costus* revealed a diversity of secondary metabolites such as sesquiterpene lactones (costunolide and dehydrocostus lactone), phenolic acids (chlorogenic acid and caffeic acid), flavonoids (quercetin and kaempferol), and alkaloids, phytosterols, lignans, tannins, triterpenes, and essential oils.[19,20] While crude extracts from *S. costus* demonstrate valuable pharmacological activity, several challenges hinder their effectiveness to be integrated into mainstream therapeutics. For example, sesquiterpenes and lipophilic flavonoids have low water solubility, resulting in low plasma concentration and minimal therapeutic effect, even at high doses.[21–23] Even when absorbed, poor permeability through biological membranes and rapid hepatic metabolism may result in short half-life and low effectiveness.[24] Polyphenols and essential oils are sensitive to pH, light, temperature, and oxidation, resulting in loss of potency upon administration or during storage.[23,25–27] Additionally, non-selective targets throughout the body could reduce the efficacy in targeted disease sites like tumors.[28] These limitations necessitate advanced delivery strategies to the delivery of *S. costus* derived compounds.

To overcome these limitations, plant extracts were incorporated into different delivery systems to improve their biological performance.[29] These innovative systems include lipid-based nanocarriers such as niosomes, liposomes and solid lipid nanoparticles which enhance the solubility of hydrophobic

Department of Chemistry, School of Sciences & Engineering, The American University in Cairo, AUC Avenue, P.O. Box 74, New Cairo 11835, Egypt. E-mail: hazzazy@aucegypt.edu; Tel: +202 2615 2559

compounds.[30,31] Polymeric systems, on the other hand, like chitosan and polycaprolactone (PCL), protect essential oils from degradation and enable controlled release of active constituents.[32,33] Additionally, metal-based nanosystems (including silver, gold, zinc, and copper oxides) are prepared using green approaches to carry natural compounds which add to their intrinsic antimicrobial or anticancer properties.[34,35]

In this review, the natural distribution and traditional use of *S. costus* was examined to highlight its ethnopharmacological relevance. *S. costus* is known for its diverse phytochemicals which contribute to a wide range of biological activities. However, despite its therapeutic promise, the use of *S. costus* in clinical applications is limited by challenges such as poor water solubility, low bioavailability, and possible toxicity in its crude form. To address these issues, this review focuses on recent progress in nanoformulation strategies, including green synthesis of metal and metal oxide nanoparticles, as well as different nanocarriers. These nanosystems are evaluated based on synthesis, physicochemical features, and biological activities to provide a comprehensive understanding of their therapeutic potentials.

2. Discovery, taxonomy, and geographical distribution of *Saussurea* species

The genus *Saussurea* belongs to the kingdom *Plantae* and is classified under clade *Asterids*. Within the Asteraceae family, *Saussurea* genus is further assigned to the subfamily *Carduoideae* and belongs to the tribe Cardueae with over four hundred species of perennials.[1,36] Additionally, the taxonomy of different species is often challenging to resolve within this genus due to frequent hybridization, morphological plasticity, and convergent evolution in high-altitude environments. To resolve the complex taxonomy of *Saussurea*, many studies have turned to study the molecular phylogenetics of these species, where they analyzed the DNA sequences to understand the evolutionary relationships among species.[2,6,37,38] For example, Wu *et al.* found that genes, such as (*CBF1*, *COR15A*, *COR47*, and *KIN1*) are upregulated, aiding the adaptation of *S. involucrate* to cold and high-altitude environments.[39] The genus *Saussurea* was named in honor of the Swiss naturalists Horace-Bénédict de Saussure based on specimens collected during 18th century.[40,41] The species of *Saussurea* exhibit broad distribution across the Northern Hemisphere including North America, Europe, Asia, and North Africa. China exhibits the highest diversity of the of this plant with an estimation of 317 species, concentrated in alpine regions such as the Hengduan Mountains and Qinghai-Tibet Plateau.[42] For example, *S. involucrata* is endemic to the Altai and Tianshan mountains,[43] while *S. minutiloba*,[42] *S. balangshanensis*,[44] and *S. medusa*[45] are found in the Hengduan mountains. In the Indian Himalayan region, 62 species of *Saussurea* are documented to hold medicinal and cultural significance such as, *S. costus* and *S. obvallata*.[4] In Mongolia around the Khangai mountains species such as *S. salicifolia* are found.[46] Additionally, in Japan and South Korea, endemic species like *S. tanquetti* and *S. japonica* are observed.[47] In Russia, particularly in Siberia, species like *S. amara* and *S. daurica* are commonly reported.[48] Beyond Asia, the genus also extends into Europe, with species like *S. pygmaea*, *S. discolor*, and *S. alpina*, inhabiting the Alps and Slovakia.[38,49] In North America, *S. weberi* and *S. americana* are distributed from Alaska through the Rocky mountains to northern California.[38] Additionally, a few *Saussurea* species were recorded in North Africa, particularly in the Atlas mountains of Algeria and Morrocco.[50,51]

3. Traditional use of *Saussurea* species

The *Saussurea* genus has a long-standing ethnomedicinal history, particularly in Asia. Several *Saussurea* species were traditionally used in different medicine systems such as Traditional Chinese Medicine (TCM), Ayurveda, Tibetan, and Korean medicine.[1,7–10] They are often administered as powders, decoctions, and oils, either alone or in polyherbal formulations. In TCM, *S. involucrate* (known as Snow Lotus) was documented in the Chinese Compendium of Materia Medica, where it was described as a remedy for arthritis, menstrual pain, and altitude sickness, highlighting its traditional use in regions of Xinjiang and Tibet.[52] Similarly, in Tibetan medicine, *S. medusa* and *S. laniceps* were traditionally used in polyherbal formulations as anti-inflammatory agent to treat cold disorders.[7]

Among the *Saussurea* genus, *S. costus* (also known as costus root) is extensively documented for its traditional use. In Ayurveda, it is referred to as Kushtha and is regarded as one of the most potent herbs for treating respiratory disorders (asthma and bronchitis), skin diseases, rheumatism, and ulcers due to its antimicrobial, anti-inflammatory, and expectorant properties.[53] Ayurvedic texts like *Sushruta Samhita* and *Charaka Samhita* described the importance of *S. costus* in formulations used for detoxification, digestive disorders, and respiratory diseases.[54] In Unani medicine, the root is valued for its ability stimulate brain activity, and improve liver and kidney functions, and is commonly prescribed for anemia, hyperglycemia, hyperlipidemia, ulcer and chronic cough.[55] Furthermore, in the Chinese Pharmacopoeia, it is recommended for managing abdominal pain, bloating, and dysentery by alleviating gastrointestinal stagnation.[56]

Recently, *S. costus* has attracted growing scientific interest due to its strong medicinal potential. Studies on its root extract have revealed a range of important pharmacological properties.[1,57,58] However, overharvesting this plant has led to a significant decline in its wild populations. As a result, the species was classified under Appendix I of the Convention on International Trade in Endangered Species of Wild Fauna and Flora (CITES), which includes species threatened with extinction.[59] This highlights the urgent need for conservation measures and the development of sustainable cultivation methods to protect this valuable medicinal plant.[57,60]

4. Bioactive metabolites of *S. costus*

A wide range of extraction methods were employed to isolate the phytoconstituents of *S. costus*, each of which generated different

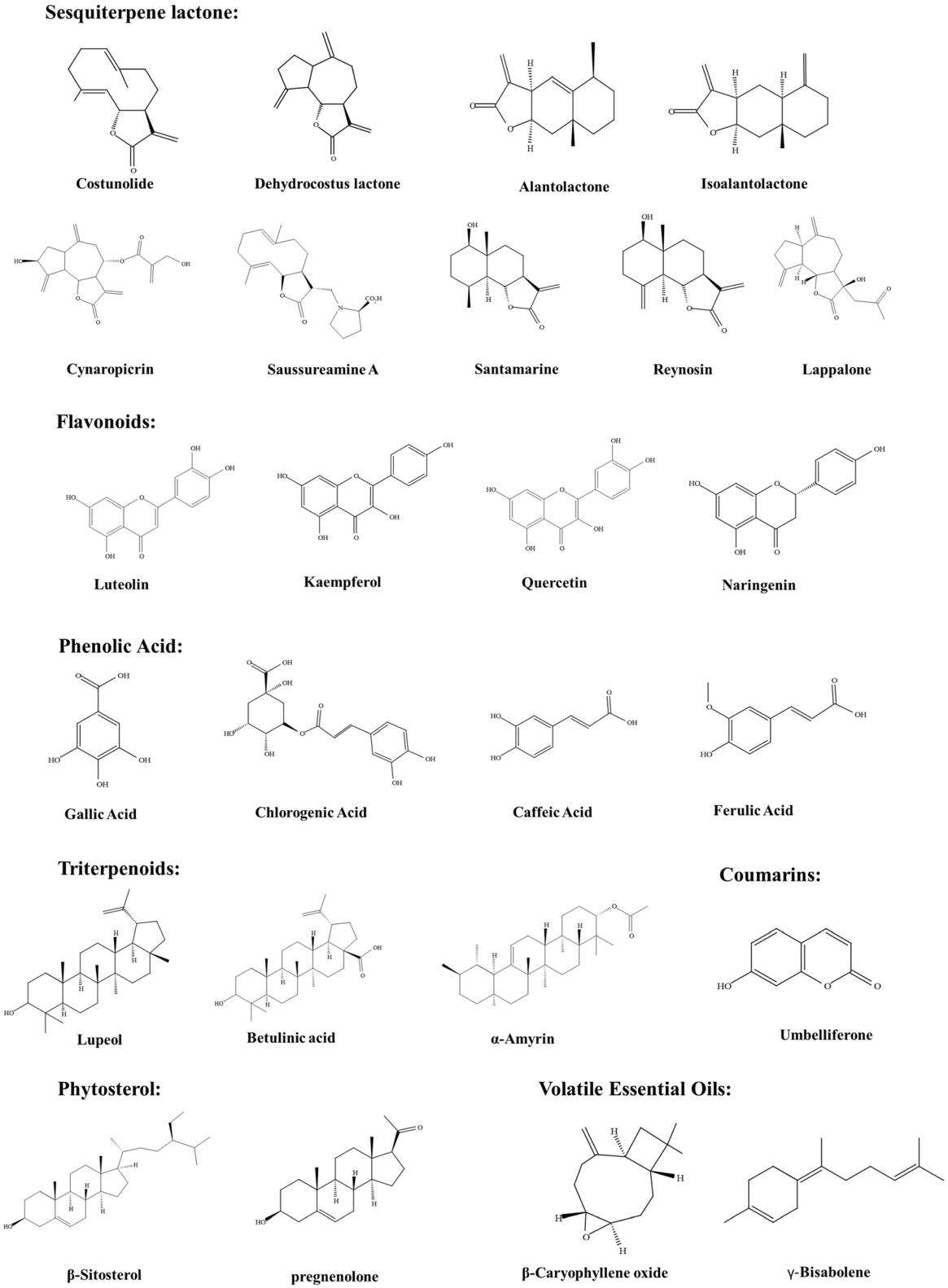

Fig. 1 Chemical structures of bioactive compounds extracted from *S. costus*.

yields and profiles of the bioactive compounds. Maceration,[57] Soxhlet extraction,[61] and percolation[62] were used to isolate key constituents using solvents like acetone, ethanol, methanol, hexane, and water. Additionally, techniques such as ultrasonic-assisted extraction,[62] microwave-assisted extraction,[63] and supercritical fluid extraction[64] have enhanced extraction selectivity, particularly for thermolabile and non-polar compounds. The phytochemical profile of *S. costus* is rich in secondary

metabolites that are pharmacologically active (Fig. 1). Among the secondary metabolites, sesquiterpene lactones such as costunolide, alantolactone, isoalantolactone, dehydrocostuslactone, and cynaropicrin are the most abundant and are primarily responsible for the antimicrobial, anti-inflammatory, antifungal, and immunomodulatory effects.[65] These are accompanied by a range of guaiane-, and germacrene-type lactones, such as saussureamines A–E, santamarine, lappalone, reynosin, epizaluzanins, arbusculin A & B, and colartin, further enhancing its therapeutic diversity.[65] The root of *S. costus* also contains notable flavonoids like luteolin, kaempferol, quercetin and its glycosides, which exhibit antioxidant and antimicrobial activities.[18,65] Other secondary constituents include phenolic acids (gallic acid, naringenin, chlorogenic acid, caffeic acid, and ferulic acid),[66] coumarins (umbelliferone),[18] lignans (sesamin),[18] alkaloids (saussurine, costine).[18] The triterpenoid profile comprises (lupeol, daucosterin, α-amyrin betulinic acid) all of which are associated with anti-inflammatory, hepatoprotective, and anticancer effects.[62,65,67] Additionally, a range of phytosterols, including (β-sitosterol, lappasterol, daucosterol, pregnenolone) have been identified, which may contribute to lipid-lowering and immunomodulatory functions.[65,68] Furthermore, *S. costus* is rich in volatile essential oils including β-caryophyllene oxide, γ-bisabolene, anethole, 1,8-cyclopentadecadiyne, and patchoulene, which have been linked to anticancer activities.[62,67,69]

5. Pharmacological activities of *S. costus* and their mechanisms of action

Many of the broad therapeutic properties of *S. costus*, as reported in traditional medicine, are now supported by pharmacological evidence. Notably, *S. costus* exhibits anti-inflammatory,[70,71] anticancer,[72] antioxidant,[73] antimicrobial,[74] antifungal,[74] hepatoprotective,[75] antidiabetic,[76] neuroprotective,[77] and immunomodulatory activities. For example, Choi *et al.* investigated the anti-inflammatory activity of *S. costus* extract in Wistar rats with benign prostatic hyperplasia (BPH), demonstrating that the *S. costus* significantly downregulated pro-inflammatory cytokines (TNF-α and IL-6) in inflamed prostate tissues. Additionally, it modulated apoptotic pathways by upregulating BAX (a pro-apoptotic protein) and downregulating BCL-2 (an anti-apoptotic protein), thereby restoring the apoptosis imbalance commonly associated with chronic inflammation in BPH.[70]

Another group evaluated the anti-inflammatory effects of *S. costus* on TNF-α and IFN-γ-induced inflammation in human keratinocyte cells. Results showed that there was downregulation of inflammatory chemokines (RANTES, MDC, TARC, and IL-8) through the inhibition of STAT1 phosphorylation, particularly by alantolactone, thereby blocking the downstream signaling pathways responsible for pro-inflammatory cytokine production.[71]

In terms of anticancer activity, *S. costus* has shown cytotoxic effects against a range of cancer cell lines, including colon (HCT116), liver (HepG2), and breast (MCF-7) cancers. In their research, Shati *et al.* reported that the *S. costus* leaf extract treated cancer cells were arrested in the G1 phase of the cell cycle, where levels of pro-apoptotic proteins increased and anti-apoptotic proteins decreased, suggesting that *S. costus* induced cancer cell death by targeting the mitochondrial pathway of programmed cell death.[72]

Elazab *et al.* investigated the protective effects of *S. costus* and *Glycyrrhiza glabra* extracts against arsenic-induced nephrotoxicity in chickens.[73] The administration of *S. costus* significantly ameliorated kidney damage caused by arsenic exposure through the activation of the Nrf2/HO-1 signaling pathway, which upregulates antioxidant enzymes such as superoxide dismutase and catalase. It also exerted anti-inflammatory effects by downregulating pro-inflammatory genes TNF-α and NF-κB, and decreased stress-related responses *via* reduced expression of heat shock proteins.[73]

The antimicrobial activity of *S. costus* against SARS-CoV-2 and *Candida albicans* was also investigated. Molecular docking analysis revealed that 12 out of 69 identified compounds were triterpenoids, of which 70% showed strong binding affinities (−7.8 to −5.6 kcal mol^{-1}) against SARS-CoV-2 targets, suggesting promising antiviral potential. Additionally, *S. costus* extract demonstrated notable antifungal activity, with *Candida albicans* being the most susceptible organism.[74]

El Gizawy *et al.* studied the hepatoprotective activity of *S. costus* extract against paracetamol-induced liver toxicity in male Wistar rats.[75] Paracetamol (acetaminophen), when administered in high doses, induces hepatotoxicity due to its metabolism into a toxic intermediate (NAPQI), which leads to liver cell apoptosis. Results showed that *S. costus* extract significantly attenuated paracetamol-induced liver injury in rats by increasing catalase activity and reducing oxidative stress markers like caspase 2 and CK18. Furthermore, *S. costus* modulated genetic markers involved in apoptosis and inflammation, including downregulation of miRNA-34a (less activation of cell death pathways) and miRNA-223 (suppress excessive inflammation), and upregulation of Hepatocyte Nuclear Factor 1 Alpha (restore metabolic homeostasis and enhance liver function), sirtuin-1 (reduce oxidative damage in liver), and (CCAAT/Enhancer-Binding Protein Alpha which supports cell regeneration and suppresses inflammatory damage).[75]

Abouelwafa *et al.* investigated the antidiabetic activity of *S. costus* extracts in a streptozotocin induced diabetic rat model.[76] The *S. costus* extracts demonstrated inhibitory activity against digestive enzymes such as α-amylase, α-glucosidase, and lipase, which are involved in carbohydrate and lipid metabolism. *S. costus* extract significantly lowered blood sugar (in terms of glucose and HbA1c levels), supported gluconeogenesis (decreased F-1,6-BP, G-6-P), and enhanced glycolysis (increased glucokinase). It also improved the lipid profile by increasing HDL and decreasing triglycerides and total cholesterol levels.[76]

Moreover, Abdel-Rahman *et al.* evaluated the neuroprotective and endocrine-modulating effects of *S. costus* root extract in male albino rats exposed to thorium-induced toxicity.[77] The cerebellum accumulated thorium caused significant oxidative damage and monoamine depletion. Pretreatment of the albino rats with *S. costus* extract significantly

enhanced the antioxidant defense system evidenced by reduced lipid peroxidation and nitric oxide levels and restored glutathione content.[77]

6. Limitations of using *S. costus* extracts in therapeutic applications

Despite the reported pharmacological activities of *S. costus*, the direct use of its free extract in medicinal formulations is limited (Fig. 2). One of the primary challenges is hydrophobicity of its bioactive compounds such as sesquiterpene lactones and flavonoids.[78,79] These constituents exhibit low dissolution in physiological fluids (blood or gastric juice), resulting in suboptimal absorption and low systemic bioavailability.[78,79] For example, costunolide, a sesquiterpene lactone that is abundant in *S. costus* extract, exhibits low water solubility estimated at approximately 9.38 mg L^{-1} at 25 °C.[80] Similarly, dehydrocostus lactone is insoluble in water, further limiting its bioavailability.[81] *S. costus* phytochemicals are also highly prone to environmental degradation. Vadaparthi *et al.* investigated on the stability of costunolide and dehydrocostus lactone in *S. costus* using liquid chromatography which exhibited significant degradation under alkaline conditions.[82] Additionally, polyphenols and essential oils degrade rapidly upon exposure to heat, oxygen, or light, reducing the shelf life and the therapeutic efficacy.[83,84] Furthermore, these compounds undergo hepatic first-pass metabolism, leading to rapid elimination. A pharmacokinetic study conducted by Peng *et al.* on dehydrocostus lactone and costunolide showed that these compounds experience rapid hepatic metabolism in rats. This necessitates higher or more frequent dosing to achieve therapeutic levels, which may increase the risk of toxicity.[85] The application of *S. costus* sesquiterpene lactones in topical formulations is challenging due to potential skin irritation. These compounds can act as haptens, binding to skin proteins and triggering immune responses. A study by Cheminat *et al.* showed that sesquiterpene lactones, can be recognized by the immune system of sensitive individuals, causing allergic reactions.[86] This could be mitigated by encapsulating *S. costus* extracts to reduce direct skin exposure and irritation.[86] Another major limitation is the lack of specificity. When administered in free form, the active constituents of *S. costus* are distributed non-selectively throughout the body.[87] Furthermore, batch-to-batch variability due to differences in plant growth conditions, harvesting methods, and extraction techniques pose challenges for standardization and reproducibility in therapeutic applications.[88] These issues collectively underscore the need for advanced formulations to optimize the therapeutic potential of *S. costus*.

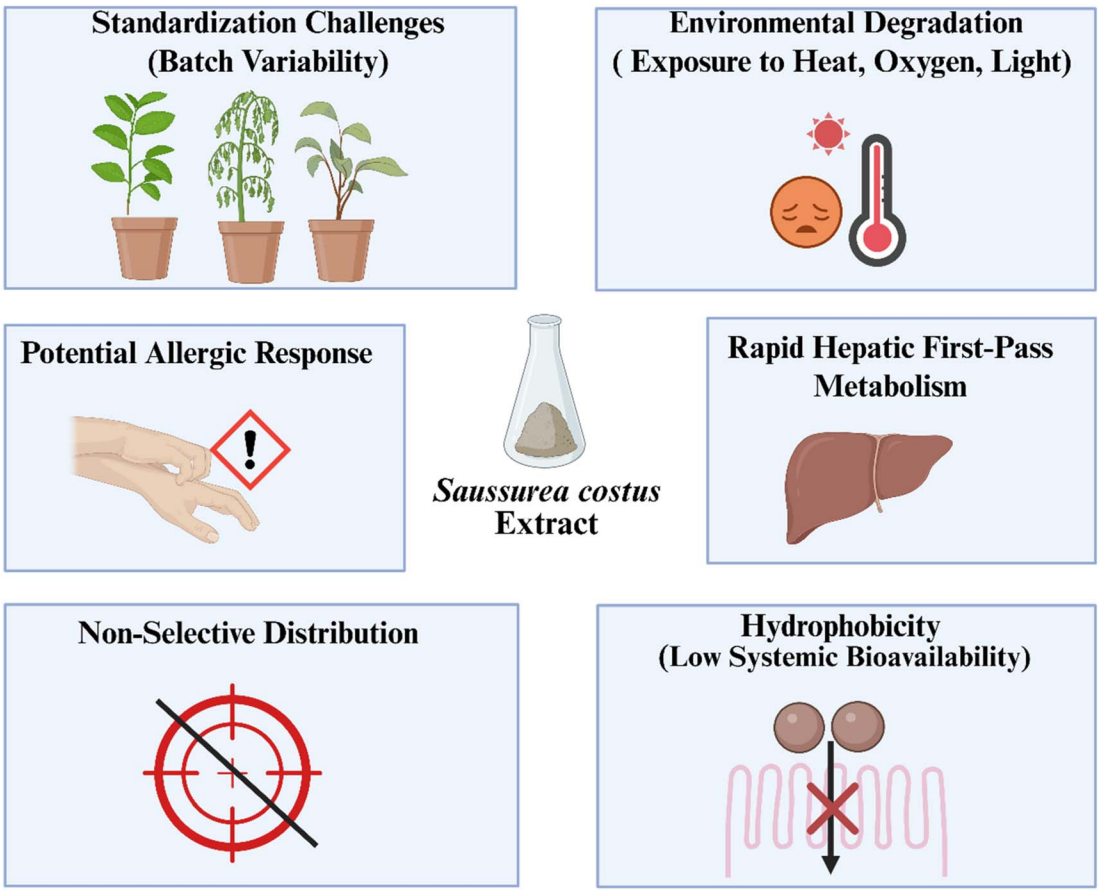

Fig. 2 Challenges limiting the therapeutic potential of free *S. costus* extract.

7. Advanced nanosystems for maximizing therapeutic potential of *S. costus*

Advanced delivery systems have emerged as effective tools to improve the delivery *S. costus*, with green synthesis and nanoformulation strategies showing considerable promise.[89–98] Plant-mediated green synthesis of metal and metal oxide nanoparticles offers a simple, sustainable route in which phytochemicals from the extract act as both reducing and capping agents, often conferring additional biological activity compared with chemically synthesized nanoparticles.[99,100] Moreover, nanoformulations such as polymeric,[94] lipid,[97] inorganic nanoparticles,[98] and nanofibers[96] can improve the bioavailability, stability and target-site accumulation of phytoconstituents while protecting them from rapid metabolism and degradation. This review presents nanosystems developed for *S. costus* and highlights how green synthesis and nanoencapsulation strategies helped overcome key limitations of the free extracts and consequently enhanced their biological activity in different biomedical applications. A structured search was conducted in PubMed (n = 19), Scopus (n = 33), and Web of Science (n = 47) to identify reports on *S. costus*/*S. lappa* formulated as metallic, polymeric, lipidic, or hybrid nanosystems. After removal of 47 duplicates, 52 records were screened. 32 were excluded (not nano, no *S. costus*, review), and 20 studies met the eligibility criteria and were included in this review. The selection process is summarized in Fig. 3.

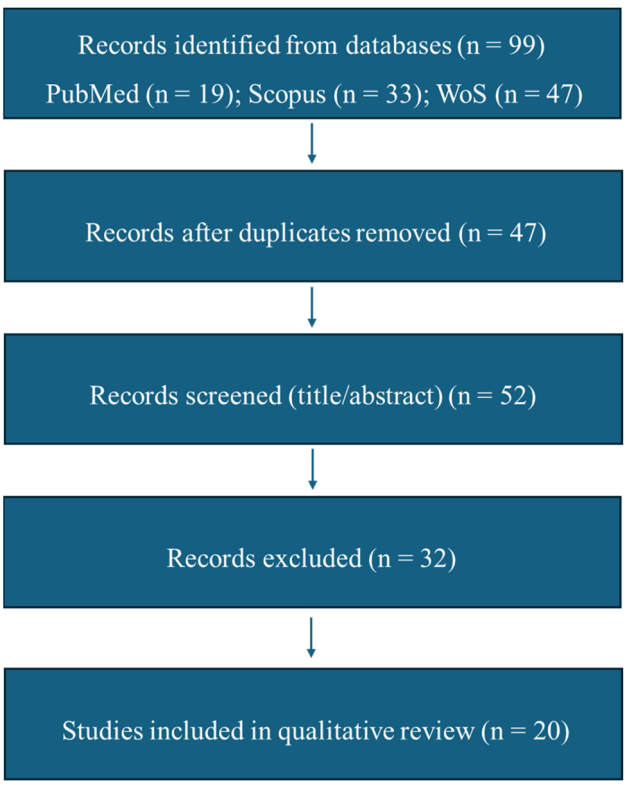

Fig. 3 PRISMA-style flow diagram for selection of *S. costus* nanoformulation studies.

7.1 Green synthesis of metal-based nanoparticles using *S. costus*

Recent studies have demonstrated the use of *S. costus* extract as a natural reducing agent for the green synthesis of metal and metal oxide nanoparticles with enhanced biological activities (Table 2).

7.1.1 Silver nanoparticles (AgNPs). Bharathi *et al.* prepared AgPNs utilizing the aqueous root extract of *S. costus* as a reducing agent and incorporated AgNPs in a chitosan hydrogel matrix and evaluated their antimicrobial activities for wound healing application.[99] Characterization of the prepared nanoparticles using transmission electron microscopy (TEM) and scanning electron microscopy (SEM) confirmed the spherical shape of the nanoparticles with a size in the range of 10–20 nm. Dynamic light scattering (DLS) showed that the diameter of the nanoparticles was 44 nm. X-ray chromatography (XRD) confirmed the crystallinity of silver (face-centered cubic), while Fourier transform infrared (FTIR) revealed functional groups from *S. costus* phytochemicals, possibly responsible for reduction of silver ions. Thermal analysis included thermogravimetric analysis (TGA) and differential scanning calorimetry (DSC). TGA indicated a weight loss occurred between 200–500 °C with a total weight loss of 49.71%, indicating the presence of organic molecules of *S. costus* extract stabilizing AgNPs. The melting point was 966.4 °C. To evaluate the biocompatibility AgNPs, MTT assay was performed on human leukemia cell lines (THP-1) for 24 h, showing an inhibitory concentration (IC_{50}) of 151.10 μg mL^{-1}. The AgNPs were then loaded into a chitosan hydrogel, showing a swelling ratio of 41% and good spreadability, with sustained release for 3 h. Five bacterial strains were used to evaluate the antimicrobial activities including *Escherichia coli* (*E. coli*), *Pseudomonas aeruginosa* (*P. aeruginosa*), *Bacillus cereus* (*B. cereus*) *Staphylococcus aureus* (*S. aureus*), and *Klebsiella pneumoniae* (*K. pneumoniae*), using agar well diffusion method. Among the tested strains, *P. aeruginosa* exhibited the highest susceptibility with an inhibition zone of 21.47 ± 0.50 mm, followed by *S. aureus* (19.97 ± 0.73 mm), *E. coli* (17.30 ± 0.03 mm), and *K. pneumoniae* (15.50 ± 0.51 mm), while *B. cereus* showed the lowest response at 11.52 ± 0.19 mm. For the *in vivo* study, *P. aeruginosa*-infected Wistar rats were treated with chitosan hydrogel-AgNPs for 15 days. This resulted in significant reduction in wound area from 518 mm^2 to 16 mm^2 with no evident bacterial load (Fig. 4). Histological analysis showed enhanced collagen and fibroblasts production in the wound. Additionally, tissue remodeling biomarkers showed a significant elevation in the treated group confirming tissue regeneration.[99]

Hijazi *et al.* utilized *S. costus* root aqueous extract to evaluate the antibacterial activity of AgNPs against different microbial strains, and their catalytic efficiency in degrading organic dyes.[101] TEM showed spherical particles of 22 nm in size. The hydrodynamic diameter of AgNPs using DLS was 66.2 nm, with polydispersity index (PDI) of 0.249, and a zeta potential of −21.57 ± 2.72 mV, indicating monodispersity of the prepared AgNPs. TGA indicated a total weight loss of 68.6%, signifying stabilization of AgNPs by organic content of *S. costus*.

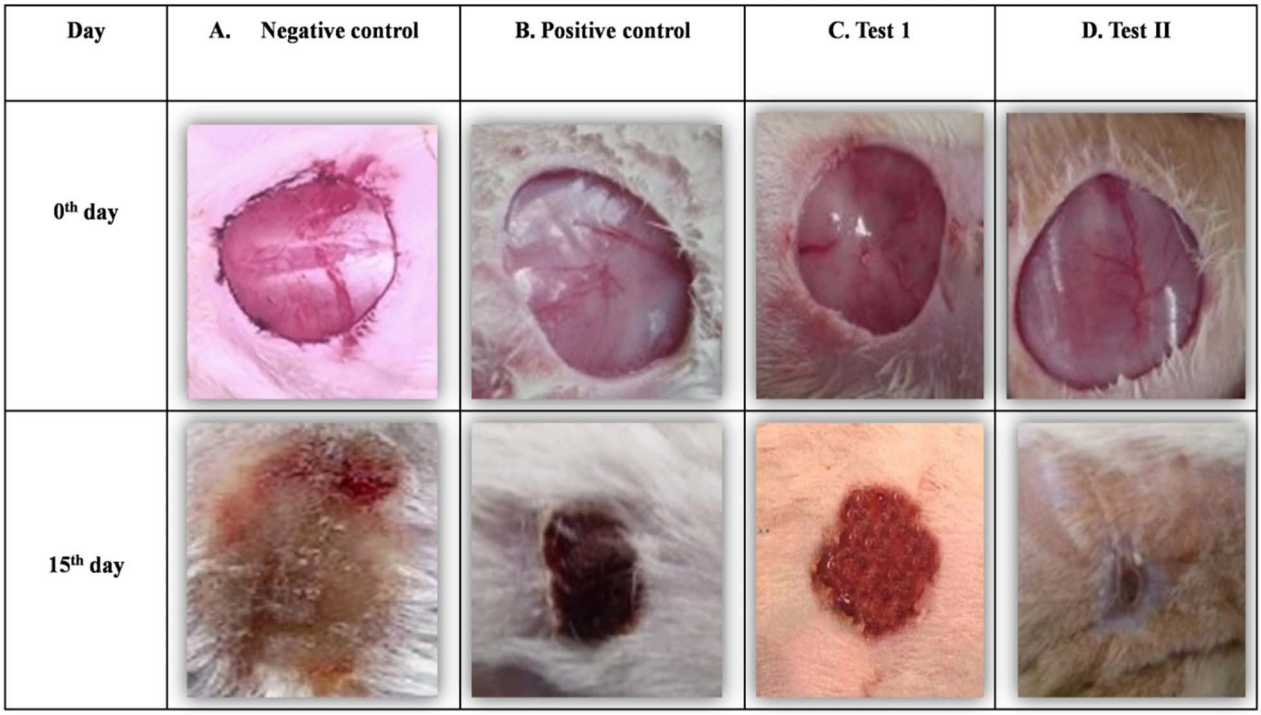

Fig. 4 Wound healing progression in *P. aeruginosa*-infected Wistar rats over a 15-day period under different treatment conditions. (A) Negative control (no treatment) exhibited delayed healing and persistent wound area. (B) Positive control group treated with silver sulfadiazine showed partial wound contraction. (C) Test I group treated with blank chitosan hydrogel displayed moderate healing. (D) Test II group treated with chitosan hydrogel-AgNPs synthesized using *S. costus* extract demonstrated significant healing, with complete wound closure (from 518 mm^2 to 16 mm^2) and absence of bacterial infection. Reproduced with permission from,[99] Springer Nature, 2021.

Photoluminescence (PL) spectroscopy confirmed the successful formation of AgNPs with excitation wavelength at 400 nm and emission wavelength at 534 nm, indicative of surface plasmon resonance (SPR) with no spectral overlap observed with either *S. costus* or the silver nitrate solution. The antibacterial efficacy of the green-synthesized silver nanoparticles was assessed against *Staphylococcus aureus* (*S. aureus*), *Klebsiella pneumoniae* (*K. pneumoniae*), *Enterococcus faecalis* (*E. faecalis*), and *Staphylococcus haemolyticus* (*S. haemolyticus*) using the agar well diffusion method. Among the tested strains, *S. haemolyticus* exhibited an inhibition zone of 15.33 ± 0.57 mm (highest susceptibility), while *E. faecalis* showed inhibition zone of 12.0 ± 0.4 mm (lowest susceptibility). The minimum inhibitory concentration (MIC) values ranged from 0.0394 to 0.158 g L^{-1}, and the minimum bactericidal concentration (MBC) values ranged from 0.0788 to 0.315 g L^{-1}. Based on the MBC/MIC ratios, the nanoparticles exhibited bacteriostatic effect (ratio = 8) against *K. pneumoniae*, bactericidal activity (ratio ≤4) against *S. aureus*, *S. haemolyticus*, and *E. faecalis*. The nanoparticles also demonstrated catalytic activity in degrading toxic dyes like safranin, methyl orange, methylene blue, Congo red, and orange G. These results highlight the potent antibacterial and catalytic activity of silver nanoparticles green-synthesized using *S. costus* extract.[101]

Another group tested the antimicrobial and antioxidant activity of AgNPs synthesized using the aqueous *S. costus* root extract.[102] SEM images revealed spherical shape of the prepared nanoparticles. XRD analysis confirmed the crystallinity of AgNPs, and the calculated crystallite size was 20.15 nm, with lattice constant of 4.086 Å. Surface plasmon resonance (SPR) peak was detected at 440 nm using UV-Vis spectroscopy, indicative of nanoparticle formation. FTIR analysis showed

Table 1 Evaluation of antioxidant and anticancer activities of L-AgNPs and R-AgNPs and their corresponding free extracts.[92]

	Leaf extract	Root extract	L-AgNPs	R-AgNPs	Ref.
DPPH (% scavenging activity)	81.0	83.5	95.3	97.7	92
ABTS (% scavenging activity)	84.7	81.0	97.7	95.3	
FRAP (% Fe^{3+} reduction)	74.7	67.2	91.9	95.6	
FRAP (mg gallic acid equivalent per L)	59.5	39.2	43.5	65.1	
MDA-MB-231 (IC50 μg mL^{-1})	86	120	56	60	
LoVo (IC50 μg mL^{-1})	74	74	50	42	
HCT-116 (IC50 μg mL^{-1})	82	82	56	60	

functional groups corresponding to flavonoids, phenols, amides, and amines, indicating successful bio-reduction of silver nitrate. The antimicrobial activity against *P. aeruginosa* and *E. coli* of AgNPs, methanol *S. costus* root extract, and aqueous *S. costus* root extract were evaluated and compared. The agar well diffusion method was utilized showing zones of inhibition of 11.0 mm against *E. coli* and 9.0 mm against *P. aeruginosa* in case of AgNPs. In comparison, the methanolic root extract alone showed moderate inhibition (9.0 mm for *P. aeruginosa* and 6.0 mm for *E. coli*), while the aqueous extract produced a 6.0 mm inhibition zone for both bacteria. Additionally, the antioxidant activity of methanolic extract was tested showing an IC_{50} value of 0.814 μg mL^{-1}, attributable to its rich content of total flavonoids (145 mg rutin equivalent per g) and total phenolics (205 mg gallic acid equivalent per g).[102]

Aqueous extracts from both *S. costus* leaves and roots were utilized to synthesize AgNPs.[92] SPR peaks was evident at 420 nm for *S. costus* root-derived AgNPs (R-AgNPs) and at 407 nm for leaf-derived nanoparticles (L-AgNPs). TEM analysis revealed smaller particle size for R-AgNPs (26 nm), while L-AgNPs had a size of 55 nm. Monodispersity of the nanoparticles was examined by DLS in which R-AgNPs exhibited PDI of 0.2578 (diameter = 50.32 nm), and for L-AgNPs, PDI was 0.1448 (diameter = 148.8 nm). Energy-dispersive X-ray spectroscopy (EDX) confirmed the phytochemical surface capping evident by signals corresponding to carbon, oxygen, and potassium in addition to strong silver peaks. Three assays, 2,2-diphenyl-1-picrylhydrazyl (DPPH), 2,2′-azino-bis(3-ethylbenzothiazoline-6-sulfonic acid) (ABTS), and ferric reducing antioxidant power (FRAP), were employed to assess the antioxidant activity of R-AgNPs and L-AgNPs (Table 1). The scavenging activity was significantly higher in AgNPs than in their corresponding plant extracts. Notably, R-AgNPs exhibited superior antioxidant activity, which can be attributed to the higher content and diversity of phenolic and flavonoid compounds in the root extract. The study also evaluated anti-inflammatory activities through the inhibition of proinflammatory enzymes, such as 5-LOX, COX-1, and PLA_2s, achieving over 99% inhibition at a concentration of 120 μg mL^{-1} for both R-AgNPs and L-AgNPs. MTT assay was utilized to evaluate the anticancer activity of the prepared nanoparticles and their free extracts against colorectal adenocarcinoma (LoVo), colorectal carcinoma (HCT-116), and triple-negative breast cancer (MDA-MB-231) cells. The results indicated enhanced antiproliferative effects of R-AgNPs and L-AgNPs compared to the free form of the extracts with IC_{50} values ranging between 42 and 60 μg mL^{-1} (Table 1). Finally, antimicrobial activity against bacteria (*E. coli*, *S. aureus*, *Bacteroides fragilis* (*B. fragilis*), and *Enterococcus faecalis* (*E. faecalis*)) and fungi (*Aspergillu niger* (*A. niger*), *Penicillium digitatum* (*P. digitatum*), and *Aspergillus oryzae* (*A. oryzae*)) was evaluated. Both AgNPs displayed a more significant antimicrobial effect than the corresponding *S. costus* aqueous extracts. L-AgNPs were the most effective, especially against *E. coli* and *E. faecalis* with an IC_{50} of 14.3 μg mL^{-1}. For the antifungal activities, L-AgNPs and R-AgNPs showed 2–3 times more potency than their free extracts. R-AgNPs were particularly potent against *A. oryzae* with IC_{50} of 2.50 μg mL^{-1}.[92]

7.1.2 Copper nanoparticles (CuNPs) and copper oxide nanoparticles (CuONPs). Kumar *et al.* synthesized CuNPs using two aqueous extracts of *Bauhinia variegata* (*B. variegata*) flower (6%) and *S. costus* flower (3%) to explore their anti-obesity, anti-diabetic, and antimicrobial activities.[103] The solution color change from blue to green indicated formation of CuNPs. The SPR peaks of CuNPs were detected using UV-Vis spectroscopy showing absorption from 280–500 nm range. DLS showed a particle size of 98.03 nm (*S. costus*) and 8.721 nm (*B. variegata*). SEM imaging of CuNPs revealed irregular shapes, surfaces, and edges of CuNPs. EDX confirmed Cu-rich composition. XRD confirmed high crystallinity of the synthesized CuNPs. Antimicrobial tests were conducted against *P. aeruginosa*, *E. coli*, *S. aureus*, and *K. pneumoniae* using agar well diffusion method. The zones of inhibitions ranged from 17 to 19 mm, comparable to conventional antibiotics like ampicillin. This antimicrobial action could be attributed to generation of reactive oxygen species (ROS) that disrupted the membrane integrity of bacteria, and the release of Cu^{2+} ions. Additionally, the presence of residual flavonoids and polyphenols from the *B. variegata* and *S. costus* extract provided a synergistic antibacterial effect. Pancreatic lipase inhibition assay was conducted to evaluate anti-obesity activity. *S. costus* derived-CuNPs showed 47.01% inhibition of pancreatic lipase (IC_{50} of 60.01 μg mL^{-1}), while *B. variegata*-mediated CuNPs revealed 59.67% inhibition of pancreatic lipase at 100 μg mL^{-1}. In terms of anti-diabetic activity, results showed strong potential for reducing post-prandial glucose levels evaluated by α-amylase inhibition assay, where the IC_{50} of *B. variegata*-mediated CuNPs was 78.06 μg mL^{-1} showing 89.02% inhibition of α-amylase and *S. costus* CuNPs had an IC_{50} = of 45.31 μg mL^{-1} with 56.45% inhibition.[103]

Another study conducted by Kolahalam *et al.* synthesized CuONPs using a mixture of *S. costus* root extract and *Ocimum sanctum* (*O. sanctum*) seeds extract as reducing agents to explore their cytotoxic effect on Chinese Hamster Ovary (CHO) cells, antibacterial, and antifungal activities.[100] UV-Vis spectroscopy revealed peaks at 270 nm corresponding to CuONPs and 500 nm related to *S. costus* and *O. sanctum*-derived compounds. The size of the CuONPs was estimated by DLS to be 103.4 ± 27.4 nm with zetapotential of +63.2 mV suggesting high stability. XRD revealed a crystallite size of 38 ± 1 nm confirming crystallinity. SEM images showed cuboidal and round particles exhibiting a size range of 40–60 nm, while EDX showed copper and oxygen peaks. Functional groups related to plant extracts including N–H, O–H, and C≡C were detected in FTIR spectrum. Thermal analysis indicated a weight loss of 22.5% due to the decomposition of organic compounds form the extracts TGA, while DSC analysis showed a strong exothermic peak at 700 °C. To assess the antimicrobial activities, different bacterial strains isolated from drinking water were used, including *Sphingobacterium thalpophilum*, *Ochrobactrum* sp., *Acinetobacter* sp., *Sphingobacterium* sp., *P. aeruginosa*, *E. coli*, and *Bacillus subtilis*, *Streptococcus aureus*, *Staphylococcus aureus*. *Staphylococcus aureus* and *Bacillus subtilis* exhibited the highest sensitivity towards CuONPs (170 ppm), both showing zones of inhibition of 3.2 ±

Table 2 Characteristics and biological activities of *S. costus*-derived metal or metal oxide nanoparticles[a]

Nanoparticle type	*S. costus* part/extract type	Characterization of nanoparticles	Reported bioactivity	Ref.
Chitosan hydrogel loaded-AgNPs	Root aqueous crude extract	-UV-Vis peak at 419 nm - Size: 10–20 nm (TEM and SEM) 44 nm (DLS) - Sustained release for 3 h Organic content: 49.71% (TGA) Melting point: ∼966 °C (DSC)	- Antibacterial with zone of inhibition from 11.52 to 21.47 mm (*S. aureus*, *B. cereus*, *E. coli*, *K. pneumoniae*) largest against *P. aeruginosa* (21.47 mm) - Wound healing: *P. aeruginosa*-infected Wistar rat model showed complete bacterial clearance by day 15 - No adverse effects on skin or systemic health	99
AgNPs	Root aqueous crude extract	UV-Vis peak at 460 nm PL emission peak at 534 nm Size: 22 nm (TEM), 66.2 nm (DLS) PDI: 0.249 Zeta potential: −21.57 mV Crystalline peaks at (111), (200), (220), (311) Weight loss: 69% (TGA)	- Antibacterial effect against *K. pneumoniae*, *S. aureus*, *S. haemolyticus*, *E. faecalis* - Lowest MIC: 0.0394 g L^{-1} (*K. pneumoniae*) - Bactericidal effect (MBC/MIC ≤4) *vs.* 3 strains; bacteriostatic *vs. K. pneumoniae* - Membrane disruption, ROS generation, Ag^{+} ion release - Catalytic degradation of dyes	101
AgNPs	Root aqueous extract	- UV-Vis peak at 440 nm - Crystallite size: 20.15 nm and lattice constant: 4.086 Å (XRD) - Spherical morphology (SEM)	- Antibacterial effect against *E. coli* (11.0 mm) and *P. aeruginosa* (9.0 mm) - Antioxidant	102
Polyvinyl alcohol (PVA) sheets loaded-AgNPs	Root methanolic (70%) crude extract	- UV-Vis peak at 422 nm - Size 45 ± 15 nm (TEM/SEM)	- Antibacterial effect against *E. coli*, *S. aureus* *Acinetobacter baumannii*, and MRSA at 1 μg mL^{-1} - High catalytic activity of 4-nitrophenol with 97% reduction in 18 min - Reusable for 8 cycles with >80% catalytic efficiency	105
AgNPs	Root and leaves aqueous crude extracts	- UV-Vis peak at 407 nm L-AgNPs and 420 nm for R-AgNPs - L-AgNPs: 55 nm (TEM), 148.8 nm (DLS), PDI: 0.1448 - R-AgNPs 26 nm (TEM), 50.32 nm (DLS), PDI: 0.2578 - EDX confirmed presence of Ag, O, C, K	- R-AgNPs exhibited superior antioxidant activity to L-AgNPs - AgNPs showed >99% inhibition of pro-inflammatory enzymes - IC_{50} for cancer cell lines (HCT-116, LoVo, MDA-MB-231) ranged 42–60 μg mL^{-1}, showing most potency against LoVo (R-AgNPs) - Antibacterial IC_{50} values: 14.3–20.65 μg mL^{-1} most effective against *E. coli* and *E. faecalis* (L-AgNPs) - Antifungal effect against *A. oryzae* with IC_{50} of 2.5 μg mL^{-1} (R-AgNPs)	92

Table 2 (*Contd.*)

Nanoparticle type	*S. costus* part/extract type	Characterization of nanoparticles	Reported bioactivity	Ref.
CuNPs	Flower aqueous crude extract	- UV-Vis peak at 280–500 nm Size: 98.03 nm (DLS) - Irregular morphology of CuNPs (SEM) - EDX confirmed presence of Cu and sulfur	- Antimicrobial effect (*P. aeruginosa*, *E. coli*, *S. aureus*, and *K. pneumoniae*). Inhibition zones of 17–19 mm - Anti-obesity: lipase inhibition reached 47.01% with IC_{50} of 60.01 μg mL^{-1} - Anti-diabetic: amylase inhibition reached 56.45% with IC_{50} of (45.31 μg mL^{-1})	103
Gold (AuNPs)	Root methanolic crude extract	- UV-Vis peaks at 500 nm - XRD peaks at 38°, 43.8°, 65° (111, 200, 220 planes) - Size:19 nm with spherical shape (TEM)	- Improved antioxidant capacity and stronger radical scavenging effects - Enhanced inhibition of digestive enzymes related to diabetes - Possible anti-Alzheimer's activity through acetylcholinesterase inhibition - Sustained anti-inflammatory potential *via* protein stabilization mechanisms - Increased cytotoxic effectiveness against liver (HepG2) and colon cancer (Caco2) cells - Induced cancer cell apoptosis and modulated gene expression favorably	106
IONPs	Root peel methanolic (50%) crude extract	- Size: 295 nm, zetapotential: +0.058 (DLS) - Spherical, prismatic, elongated particles (SEM/TEM)	- Antimicrobial activity against *P. aeruginosa*, *E. coli*, *Staphylococcus* sp - Morphological damage to IONPs-treated *E. coli via* membrane disruption	104
Zinc oxide (ZnO NPs)	Root methanolic crude extract	- UV-Vis peak 430 nm - Hexagonal shape of ZnO NPs (SEM) - DLS: size: 123.5 nm, zetapotential of −99.9 mV - EDX confirmed presence of Zn and O	- Strong antibacterial activity: 3.7 mm inhibition zone for *E. coli* and 3.5 mm for *P. aeruginosa* - Antifungal activity against *Meyerozyma caribbica* and *Rhizopus oryzae* (inhibition zone of 2.9 mm for both) - Cytotoxicity (MTT assay) against CHO cell line with IC_{50} of 3.16 μg mL^{-1}	107
MgO NPs	Root methanolic crude extract (Qust al-Hindi and Qust al-Bahri)	- UV-Vis peaks at 250 and 320 nm - Crystallite size (XRD): 30–34 nm - Uniform cubic morphology (SEM/TEM) - DLS: size: 20–100 nm, zeta potential: −20.5 mV	- Significant antibacterial effect (16 mm against *P. aeruginosa*) - Strong antifungal activity (20 mm against *C. tropicalis*) - Dose-dependent cytotoxicity on MCF-7 (IC_{50} = 52.1–67.3%) - 92% methylene blue dye degradation under UV by Qust al-Bahri-derived MgO NPs	93
PdNPs	Root aqueous crude extract	- UV-Vis peaks at 350 nm - DLS: zeta potential: −10.6 Mv - Size: 1.9–17.6 ± 1.2 nm and spherical shape (TEM) - EDX confirmed presence of Pd, C, O	- Enhanced antimicrobial activity compared to free extract - Antioxidant IC_{50} of 90 μg mL^{-1} - AChE/BChE inhibition 79.23%/76.13% - NO inhibition in RAW 264.7 cells by 7.84%	90

Table 2 (*Contd.*)

Nanoparticle type	*S. costus* part/extract type	Characterization of nanoparticles	Reported bioactivity	Ref.
			- Effective cytotoxicity against HCT-116 (IC_{50} 7.8 μg mL^{-1}), HepG2 (11.8 μg mL^{-1}), and MCF-7 (26.7 μg mL^{-1})	
CuO NPs	Mixture of *S. costus* root (methnolic) and *O. sanctum* seed aqueous crude extracts	- UV-Vis peak at 27 (CuO NPs) and 500 nm (phytochemicals) - Size: 40–60 nm with aggregated rough surfaces (SEM) - Size: 103.4 nm and zetapotential: 63.2 mV (DLS) - EDX confirmed presence Cu and O - Crystallite size 38 nm - Weight loss: 22.5% (organic content), stable up to 800 °C (TGA/DSC)	- Strong antibacterial activity (3.2 mm zone for *S. aureus* and *B. subtilis*) - Effective antifungal activity (2.8 mm zone for *Meyerozyma guilliermondii*) - Cytotoxic effect (MTT assay) on CHO cells with IC_{50} of 4.14 μg mL^{-1} - Biological activity attributed to ROS generation, Cu^{2+} release, and membrane damage	100
Titanium oxide (TiO_2)/ZnO nanocomposite coated by Cu(II) complex of di-Schiff bases	Root aqueous crude extract was used to produce TiO_2	- XRD: anatase TiO_2 and wurtzite ZnO, some ZnO peaks weakened after coating (amorphous organic shell), no lattice shift - TEM/SEM: irregular/spherical agglomerates about 40–100 nm, coated sample shows thicker outer layer - EDX: Ti, Zn, O plus C, N, Cu after coating - TGA: coated nanocomposite more thermally stable than the free complex - No EE% or release data reported	- Antibacterial effect (agar diffusion, 5 μg mL^{-1}) after 3 days gave 30 mm *vs. Serratia marcescens*, 30 mm *vs. E. coli*, 34 mm *vs. S. aureus* (all much higher than bare TiO_2/ZnO with ≤7 mm) - Antifungal activity with clear inhibition of *C. albicans*, *A. flavus*, *Trichophyton rubrum* - *S. costus* phytochemicals create a reactive/organic surface on TiO_2/ZnO, allowing uniform fixing of the copper(II) di-Schiff base complex, synergizing its antimicrobial activity	108

[a] Abbreviations: AChE: acetylcholinesterase; AgNPs: silver nanoparticles; AuNPs: gold nanoparticles; BChE: butyrylcholinesterase; CHO: Chinese hamster ovary; CuNPs: copper nanoparticles; CuO NPs: copper oxide nanoparticles; DLS: dynamic light scattering; DSC: differential scanning calorimetry; EDX: energy-dispersive X-ray spectroscopy; IC_{50}: half-maximal inhibitory concentration; IONPs: iron oxide nanoparticles; MCF-7: Michigan Cancer Foundation-7 cell line; MgO NPs: magnesium oxide nanoparticles; MRSA: methicillin-resistant *Staphylococcus aureus*; MTT: 3-(4,5-dimethylthiazol-2-yl)-2,5-diphenyl tetrazolium bromide assay; PDI: polydispersity index; PdNPs: palladium nanoparticles; PL: photoluminescence; ROS: reactive oxygen species; R-AgNPs: root-extract silver nanoparticles; SEM: scanning electron microscopy; TEM: transmission electron microscopy; TGA: thermogravimetric analysis; UV-Vis: ultraviolet-visible spectroscopy; XRD: X-ray diffraction; ZnO NPs: zinc oxide nanoparticles.

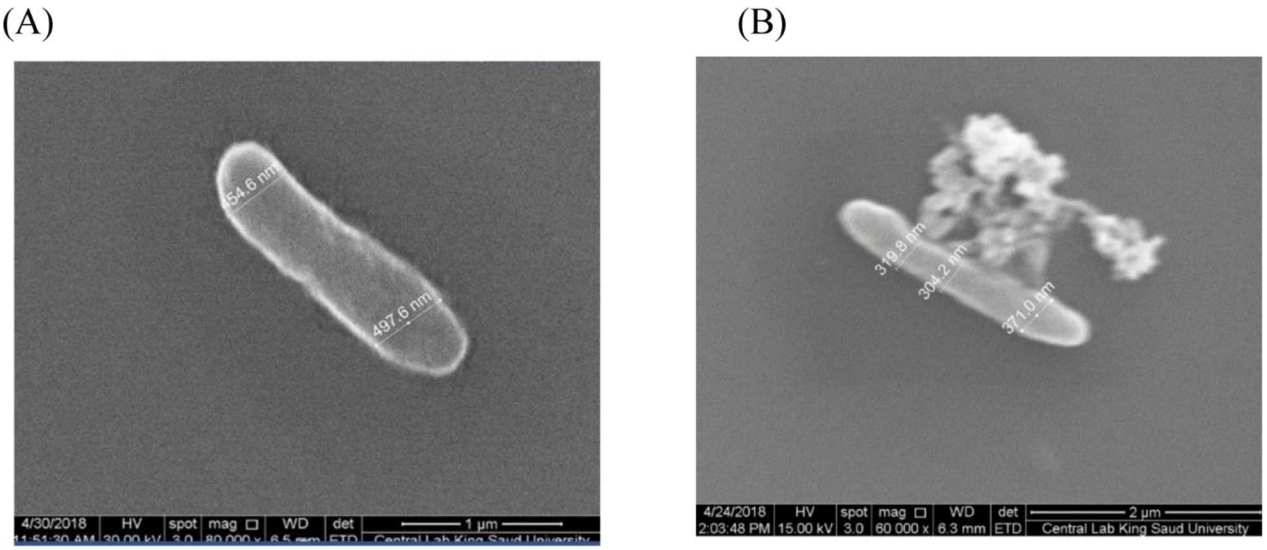

Fig. 5 SEM imaging of untreated *E. coli* (left) *vs. S. costus* -IONPs-treated *E. coli* (right). (A) Untreated *E. coli* displaying intact rod-shaped structure with typical cell dimensions. (B) IONPs-treated *E. coli* showing clear signs of membrane damage and reduced cell diameter and length.[104] Copyright license CC BY 4.0.

0.03 and 3.2 ± 0.14 mm, respectively. *P. aeruginosa* and *E. coli* showed zones of inhibition of 2.9 ± 0.08 mm and 2.7 ± 0.05 mm, respectively. The least sensitive strains were *Streptococcus aureus* (2.0 ± 0.02 mm) and *Sphingobacterium thalpophilum* (2.2 ± 0.04 mm). Antifungal properties were tested against 8 fungal strains including *Meyerozyma guilliermondii*, *Fusarium oxysporium*, *Rhizopus oryzae*, *Aspergillus flavus*, *Meyerozyma caribbica*, *Aspergillus oryzae*, and *Aspergillus niger*, and *Trichoderma asperellum*. Best antifungal activity was induced by 170 ppm of CuONPs, with reported zones of inhibition of 2.8 ± 0.05 mm and 2.7 ± 0.12 mm for *Meyerozyma guilliermondii* and *Meyerozyma caribbica*, respectively. *Fusarium oxysporium*, *Rhizopus oryzae*, and *Aspergillus flavus* showed zones of 2.0–2.1 mm. The least sensitive strains were *Aspergillus oryzae* and *Aspergillus niger*. MTT assay was conducted on CHO cell line and revealed an IC_{50} value of 4.14 μg mL^{-1} following a dose-dependent decrease in cell viability. The mechanism of inhibition includes ROS generation, metal ion release, and membrane interaction.[100]

7.1.3 Iron oxide nanoparticles (IONPs). Al-brahim biosynthesized IONPs using aqueous extract of *S. costus* root and iron salts $FeCl_2$: $FeCl_3$ (2 : 1).[104] The solution color change from yellow to dark brown indicated the formation of IONPs. TEM and SEM revealed that IONPs exhibited spherical, elongated, or prismatic curved shapes. The average size of the prepared nanoparticles was 295 nm with zetapotential of +0.058 mV. For antimicrobial evaluation of *S. costus*-derived IONPs, agar well diffusion method was utilized against bacterial strains (*Staphylococcus* sp., *B. subtilis*, *K. pneumoniae*, *Shigella* sp., *P. aeruginosa*, and *E. coli*) and fungal strains (*Aspergillus niger*, *Alternaria* sp., and *Rhizopus* sp.). *P. aeruginosa*, *Staphylococcus* sp., *E. coli*, *Shigella* sp., and *Aspergillus niger* showed inhibition zones of 11, 9, 9, 6, and 5 mm, respectively. Comparative tests also showed that IONPs had higher inhibitory effects than either the *S. costus* free extract or Fe ions alone. SEM imaging revealed morphological differences between untreated and IONPs-treated *E. coli* (Fig. 5). While the untreated cells appeared smooth with typical rod-shaped morphology, the IONPs-treated *E. coli* showed structural damage, including membrane distortion, surface corrugation, and reduction in both cell length and diameter. These alterations suggest that the IONPs compromised the bacterial cell wall integrity, supporting membrane disruption as a primary mechanism of antimicrobial action of *S. costus* -derived IONPs.[104]

7.1.4 Magnesium oxide nanoparticles (MgO NPs). Amina *et al.* biosynthesized MgO NPs using methanolic root of *S. costus* and evaluated their antimicrobial, antifungal, and anticancer activities.[93] Two varieties of *S. costus* were used one is Qust al-Hindi obtained from Indian woods (mountains) and the other is Qust al-Bahri retrieved from sea (coastal regions). The change of yellow colored aqueous solution of Mg $(NO_3)_2$ to dark brown confirmed the formation of MgO NPs. UV-Vis spectroscopy showed SPR peaks at 320 nm (indicating MgO NPs formation) and 250 nm (possibly due to phytochemical constituents). FTIR analysis indicated the presence of functional groups such as –OH, C=O, and Mg–O, while XRD revealed crystalline structure with particle sizes of approximately 30 nm and 34 nm for MgO NPs prepared using Qust al-Hindi and Qust al-Bahri, respectively, as confirmed by SEM and TEM imaging. DLS confirmed the colloidal stability of the nanoparticles (−20.5 mV). EDX confirmed the presence of Mg and oxygen.

Antimicrobial activity was performed using agar well diffusion method against *B. subtilis*, *P. aeruginosa*, *S. aureus*, and *E. coli*. MgO NPs synthesized from Qust al-Bahri (35 μg mL^{-1}), showed strong antibacterial activity, most effective against *P. aeruginosa* (zone of 16 mm), followed by *E. coli* (15 mm), *S. aureus* (14 mm) and *B. subtilis* (10 mm). In contrast, Qust al-Hindi -derived MgO NPs were only effective against *B. subtilis*

(17 mm) and *E. coli* (8 mm), showing no activity against *S. aureus* and *P. aeruginosa*. Additionally, the MIC of Qust al-Bahri-MgO NPs for both *E. coli* and *P. aeruginosa* was 320 μg mL^{-1}, while the MBC was 320 μg mL^{-1} for *E. coli* and 1280 μg mL^{-1} for *P. aeruginosa*, suggesting strong bactericidal potential, particularly against *E. coli*. SEM imaging further confirmed bacterial cell wall disruption and morphological deformation in treated samples (Fig. 6).[93]

In terms of antifungal activity, Qust al-Hindi -derived MgO NPs exhibited more potent effects than Qust al-Bahri. At 35 μg mL^{-1}, they produced inhibition zones of 20 mm and 19 mm against *Candida tropicalis* and *Candida glabrata*, respectively. Qust al-Bahri -MgO NPs were active only against *C. tropicalis* (20 mm), with no effect on *C. glabrata*. The antifungal mechanism likely involves ROS-mediated oxidative stress and disruption of fungal membrane integrity.[93]

To assess the anticancer activity of MgO NPs, MTT assay was conducted on breast cancer cells (MCF-7). The IC_{50} values were 67.3% for Qust al-Bahri -MgO NPs and 52.1% for Qust al-Hindi-MgO NPs. Microscopic examination showed morphological changes in treated cells, including shrinkage, chromatin condensation, and membrane blebbing. The morphological evidence was further confirmed by LDH assay, which demonstrated increased enzyme release confirming cytotoxic damage. DNA fragmentation assay revealed fragmentation patterns in Mg ONPs-treated cells, suggesting apoptosis induction. Moreover, intracellular ROS quantification *via* fluorescence microscopy demonstrated a significant rise in ROS levels in treated cells, supporting the hypothesis that oxidative stress was a primary driver of apoptosis. Additional confirmation came from Rhodamine 123 staining, which showed loss of mitochondrial membrane potential, further implicating the apoptotic pathway. Acridine orange/ethidium bromide (AO/EtBr) dual staining was employed to differentiate between viable, early apoptotic, late apoptotic, and necrotic cells. MgO NPs-treated cells showed an 84.3 ± 0.01% apoptotic population compared to only 8.3 ± 0.7% in the untreated group, and 65.4 ± 0.06% in paclitaxel-treated cells. Additionally, DAPI staining revealed nuclear condensation and fragmentation in treated cells, further validating apoptotic cell death. A scratch assay demonstrated that MgO NPs significantly impaired MCF-7 cell migration and delayed wound closure, indicating strong anti-proliferative and antimigratory effects that could help limit tumor growth and metastasis. Finally, MgO NPs also exhibited strong photocatalytic activity against methylene blue dye, with degradation efficiencies of 92% (Qust al-Bahri) and 59% (Qust al-Hindi) after 1 h of UV exposure, demonstrating their potential in environmental and therapeutic applications.[93]

7.1.5 Palladium nanoparticles (PdNPs). Al-Radadi utilized the aqueous root extract of *S. costus* to reduce $PdCl_2$ into palladium nanoparticles and explored their biomedical applications including antibacterial, antioxidant, anti-inflammatory, anti-Alzheimer's, and anticancer activities.[90] The successful formation of PdNPs was confirmed by the color change from

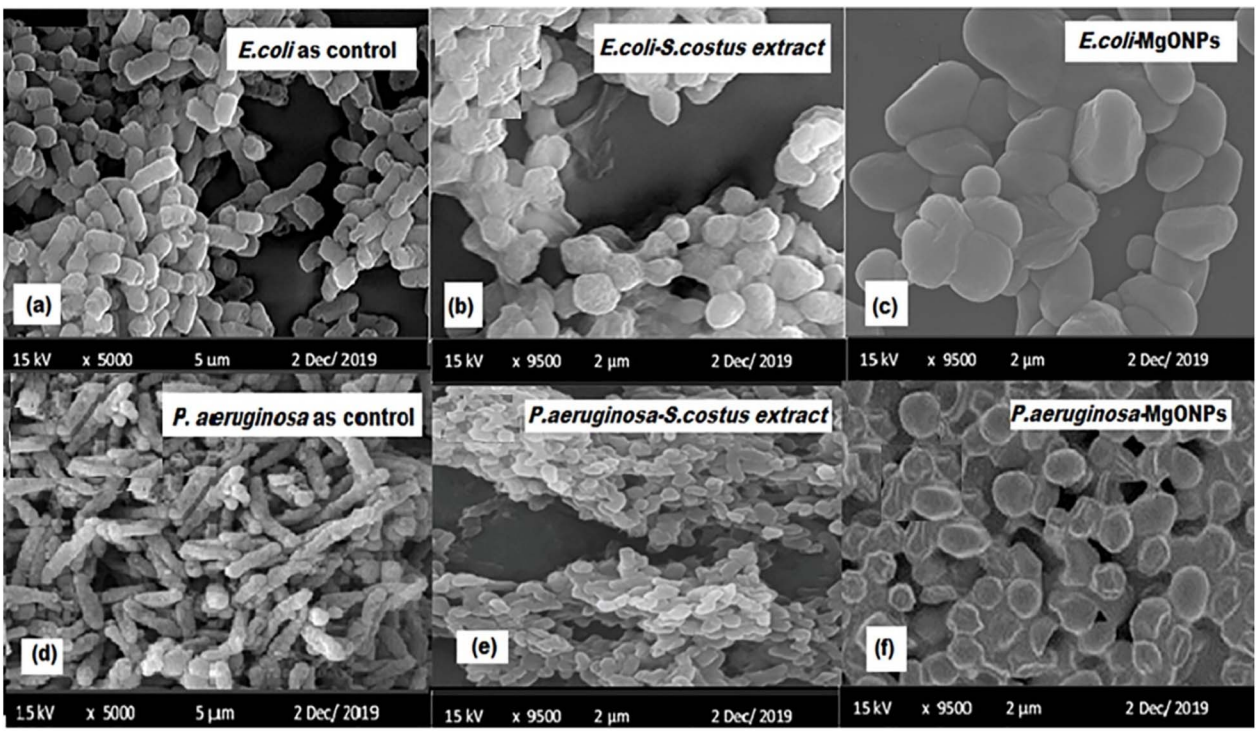

Fig. 6 SEM images illustrating the morphological changes in *E. coli* and *P. aeruginosa* upon treatment with Qust al-Bahri -mediated MgO NPs. (a) Untreated *E. coli* (control) showing rod-shaped morphology, (b) *E. coli* treated with Qust al-Bahri extract exhibiting partial surface disruption, (c) *E. coli* treated with MgO NPs displaying significant morphological deformation and membrane damage. (d) Untreated *P. aeruginosa* (control), (e) *P. aeruginosa* treated with Qust al-Bahri extract showing moderate surface changes, (f) *P. aeruginosa* treated with Qust al-Bahri-MgO NPs revealing extensive structural disruption and cell wall lysis.[93] Copyright license CC BY 4.0.

yellow ($PdCl_2$) to dark brown (PdNPs). SPR peak at 350 nm indicated Pd^0 formation. PdNPs had a diameter range of 1.9 nm to 17.6 ± 1.2 nm and spherical shape (TEM). Zeta potential analysis showed zeta potential of −10.6 mV, suggesting moderate colloidal stability. FTIR analysis identified functional group peaks at 554.30 cm^{-1} (Pd–O), 3442 cm^{-1} (hydroxyl), 2083 cm^{-1} (alkyne), and 1635 cm^{-1} (amide). Face-centered cubic crystalline structure was determined using XRD with a crystallite size of 2.88 nm. EDX confirmed the presence carbon, oxygen, and nitrogen from the plant extract as well as the Pd, while X-ray photoelectron spectroscopy (XPS) confirmed elemental palladium (Pd^0) with Pd3d peaks at 340.89 and 335.63 eV. Antimicrobial assessment was conducted against *S. aureus*, *B. subtilis*, *E. coli*, and *P. aeruginosa*, using agar well diffusion method. Zones of inhibition for *S. costus*-derived PdNPs and the free extract (at 100 μg mL^{-1}) were 22 ± 0.5 mm and 16 ± 0.1 mm (*S. aureus*), 23 ± 0.1 mm and 18 ± 0.0 mm (*B. subtilis*), 22 ± 0.3 mm and 17 ± 0.0 mm (*E. coli*), and 19 ± 0.4 mm and 15 ± 0.0 mm (*P. aeruginosa*), respectively. Furthermore, the antioxidant effect of *S. costus*-mediated PdNPs, assessed by DPPH and ABTS, was superior to the free extract, showing IC_{50} values of 90 μg mL^{-1}. This could be attributed to the high phenolic and flavonoid content in the *S. costus* and the increased surface area of the PdNPs, promoting efficient electron donation to neutralize free radicals. Furthermore, inhibition of acetylcholinesterase (AChE) and butyrylcholinesterase (BChE) implicated in Alzheimer's disease was also assessed. At 400 mg mL^{-1}, the inhibition rates were 79.23 ± 1.11% for AChE and 76.13 ± 0.43% for BChE, indicating the ability of *S. costus*-PdNPs to modulate cholinergic activity. The anti-inflammatory potential was evaluated using the Griess assay where PdNPs reduced nitric oxide production by 7.84% in LPS-stimulated murine macrophage (RAW 264.7) cells. Finally, anticancer activity against different cell lines HCT-116 (colon), HepG2 (liver), and MCF-7 (breast) was assessed using MTT assay. *S. costus*-PdNPs showed selective cytotoxicity towards tumor cells due to ROS production and apoptosis induction. The MTT assay on *S. costus*-PdNPs revealed IC_{50} values of 7.8 μg mL^{-1} (HCT-116), 11.8 μg mL^{-1} (HepG2), and 26.7 μg mL^{-1} (MCF-7), which are much lower than IC_{50} values of the free *S. costus* extracts (82.5–114.6 μg mL^{-1}). *S. costus*-PdNPs showed enhanced biomedical activities compared to free extract.[90]

7.2 Nanoformulations of *S. costus* extract

S. costus extract were incorporated into nanocarriers, such as polymeric, lipid-based nanoparticles, and inorganic nanocarriers as well as electrospun nanofibers to improve its therapeutic efficacy by enhancing bioavailability and increasing its overall stability. The following subsection covers different nanoformulations encapsulating *S. costus* extract and investigates their biological activities (Table 3).

7.2.1 Polymer-based nanoparticles. Alshubaily incorporated *S. costus* root ethanolic extract into fungal-derived chitosan (FCS) and tested their antifungal and antimicrobial activities.[89] FCS was isolated from *Aspergillus niger mycelia* using alkaline deacetylation and acidic solubilization methods. *S. costus*-loaded FCS was prepared *via* ionic gelation using sodium tripolyphosphate as a cross-linker. TEM imaging showed spherical morphology and a particle size of 48 nm. DLS analysis revealed a zeta potential of +3.28 mV, indicating good colloidal stability. FTIR analysis confirmed strong interactions between *S. costus* and FCS. To evaluate their antimycotic activity, disc diffusion and MIC assays were utilized against standard and drug-resistant *Candida albicans* and *Candida glabrata*. *S. costus*-loaded FCS exerted the highest antifungal activity against all strains in comparison to free *S. costus* and FCS. The zones of inhibition of *S. costus*-loaded FCS against all fungal strains ranged from 13.8 ± 0.7–11.1 ± 1.0 mm. Furthermore, *S. costus*-loaded FCS showed an MIC range of 1.75–3 mg mL^{-1}, lower than both free FCS and *S. costus*. Morphological changes in the treated yeast cells with their respective MICs were assessed using SEM imaging. *Candida* cells began showing membrane swelling and deformation after 6 h of treatment. By 12 h, most cells exhibited severe membrane rupture, loss of structural integrity, and lysis.[89]

Milad *et al.* examined the immunological and anti-inflammatory activities of *S. costus*-loaded chitosan nanoparticles (*S. costus*-CS NPs) in dexamethasone immunosuppressed male rats.[91] The study compared the immunomodulatory effects of *S. costus*, *Moringa oleifera*, *Ziziphus spina-christi*, and their CS nano-conjugates. Free CS nanoparticles exhibited small size (46.21 ± 28.75 nm), compared to *S. costus*-loaded CS (924 ± 112.6 nm), while maintaining a favorable positive zeta potential (+39.4 ± 7.04 mV). FTIR analysis revealed functional group interactions between *S. costus* and CS, with characteristic shifts in amide, carboxyl, and aromatic bands, confirming their successful conjugation. EE% for the *S. costus*-CS NPs system was determined by a direct method where the loaded nanoparticles were precipitated at pH 9, centrifuged, the pellet redissolved in 1% acetic acid, and EE% was calculated to be 50.09%. This value was comparable to that of *Ziziphus*-CS NPs (49.98%) and only slightly lower than that of *Moringa*-CS NPs (66.14%), demonstrating that *S. costus* can be efficiently incorporated into the chitosan nanocarrier. *In vitro* cytotoxicity of *S. costus*-CS NPs was evaluated using the water-soluble tetrazolium (WST-1) viability assay. *S. costus*-CS NPs exhibited no cytotoxic effects on human lung fibroblast (WI-38) and human embryonic kidney (HEK-293) cell lines at the tested concentration (100 μg mL^{-1}), similar to *Moringa*-CS and *Ziziphus*-CS formulations. Furthermore, *S. costus*-CS NPs were administered orally in dexamethasone-induced immunosuppressed male rats for 28 days. The *S. costus*-CS NPs-treated group showed elevation of total leukocyte count (at day 14 and day 28) and complement protein C3 compared to immunosuppressed rats, with a higher increase in C3 than that in *Ziziphus*-CS NPs, reflecting a robust activation of the complement cascade. In general, plant extract-CS conjugates induced higher TLC and C3 responses than the corresponding free extracts; accordingly, *S. costus*-CS NPs produced a more pronounced enhancement of leukocyte counts and C3 levels than free *S. costus* extract, particularly at earlier time points, indicating that nanoencapsulation amplifies the immunostimulatory effect of the traditional extract. C4 also

Table 3 Characteristics and biological activities of *S. costus* polymeric nanosystems[a]

Nanosystem	*S. costus* part/extract type	Characteristics	Reported bioactivity	Ref.
FCS	Root ethanolic (70%) crude extract	- Size: 48 nm (TEM, spherical) - Zeta potential: +3.28 mV (high stability) - EE%: NR	- *S. costus* -loaded FCS outperformed the antimycotic activity of both free *S. costus* and FCS - *S. costus* -loaded FCS showed the highest zone of inhibition (13.8 mm for standard *C. albicans*) and lowest MIC (1.75 mg mL^{-1}) - SEM imaging of treated *Candida* confirmed cell wall lysis after 6–12 h of exposure	89
CS	Root ethanolic (70%) crude extract	- Size: 924 ± 112.6 nm Morphology: spherical (TEM) - Zeta potential: +39.4 ± 7.04 mV - EE%: 50.09 (direct method)	- Immunostimulatory activity in dexamethasone-induced immunosuppressed rats - Significant increase in TLC, C3, C4, IFN-γ - Decrease in TNF-α - Ki-67 upregulation - Normal liver and kidney function -No cytotoxicity up to 5 mg mL^{-1}	91
PMMA	Root essential oils	- DLS: size: 145 nm, PDI: 0.18, zeta potential: +45 mV - Spherical morphology (TEM) - EE%: NR	- Non-cytotoxic at ≤25 μg mL^{-1} (A549 cells) - Anti-inflammatory effect: reduced TNF-α, GM-CSF, IL-1β and MMP-9 levels - Antidiabetic effect: IC_{50} for α-amylase was 22.9 μg mL^{-1} and for α-glucosidase 75.8 μg mL^{-1} - Cholinergic modulation: IC_{50} for AchE and BChE were 25.0 and 14.9 μg mL^{-1}, respectively	94
Eudragit® RS100	Root ethanolic crude extract	- DLS: size (119.7 nm), PDI (0.182) - EE%: NR	- Significant anti-inflammatory effect in a *P. gingivalis* periodontitis rat model - Day-2 changes were not significant - NF-κB and TNF-α reduced significantly by day 5	95
Eudragit® RS100	Root ethanolic crude extract	- Hydrodynamic size: 119.7 nm - EE%: NR	- Anticancer & antiproliferative activity - Inhibition of HeLa (cervical cancer) showed a dose-dependent with 50–60% viability with IC_{50} of 81.80 μg mL^{-1} - Proliferation of SHED (human dental pulp stem cells) showed a significant decrease at 12.5 μg mL^{-1} across 24/48/72 h	109
PCL-GL nanofibers	Root ethanolic (100%) crude extract	- Diameter: 253 nm (SEM) - Water contact angle: 54.6° (hydrophilic) - Controlled release: 45.99% release over 7 days - EE%: NR	- High antimicrobial activity (log reduction 7) - DPPH scavenging of 86.4% - Biocompatible with HSF cells - *In vivo* enhanced wound closure in male albino rats by 82.2% - Significant collagen deposition, downregulation of IL-6, and upregulation of BAX and MMP-3	96

Table 3 (*Contd.*)

Nanosystem	*S. costus* part/extract type	Characteristics	Reported bioactivity	Ref.
Bilosome	Costunolide	- DLS (size of 119.7 ± 3.63 nm) - EE%: 63.4 ± 3.59%	- Costunolide-loaded bilosomes showed greater anticancer potency than free costunolide in LS174T cells and maintained a more favorable profile relative to the blank carrier in normal colonic cells, supporting improved selectivity - Nanoformulation drove apoptosis (sub-G1 accumulation) and produced a pro-apoptotic gene expression. It also triggered oxidative stress and mitochondrial pathway activation	97
Silica coated with methacrylic acid	Costunolide	- Pore size: 10 nm (TEM); – drug loading: 30.5 ± 2.45% (HPLC) - Acid shielding at pH 1.0, rapid release at pH 6.8 - XRD/DSC confirmed the crystallinity of costunolide - EE%: NR	- Blank nanoparticles were biocompatible (LX-2 cells) - Loaded + coated particles suppressed TGF-β1, MMP2, α-SMA, COL1A1 more than free drug in water - *In vivo* model showed that at $\frac{1}{2}$ the dose, loaded + coated particles reduced necrosis and collagen, and improved ALT/AST more than free drug	98

[a] Abbreviations: AchE: acetylcholinesterase; BAX: Bcl-2-associated X protein; BChE: butyrylcholinesterase; C3: complement component 3; C4: complement component 4; CS: chitosan; DLS: dynamic light scattering; DPPH: 2,2-diphenyl-1-picrylhydrazyl; FCS: fungal chitosan; GM-CSF: granulocyte-macrophage colony-stimulating factor; HSF cells: human skin fibroblast cells; IFN-γ: interferon gamma; IL-1β: interleukin-1 beta; IL-6: interleukin-6; Ki-67: proliferation marker protein; MMP-3: matrix metalloproteinase-3; MMP-9: matrix metalloproteinase-9; MIC: minimum inhibitory concentration; PCL–GL: polycaprolactone–gelatin; PDI: polydispersity index; PMMA: poly(methyl methacrylate); SEM: scanning electron microscopy; TEM: transmission electron microscopy; TLC: total leukocyte count; TNF-α: tumor necrosis factor-alpha.

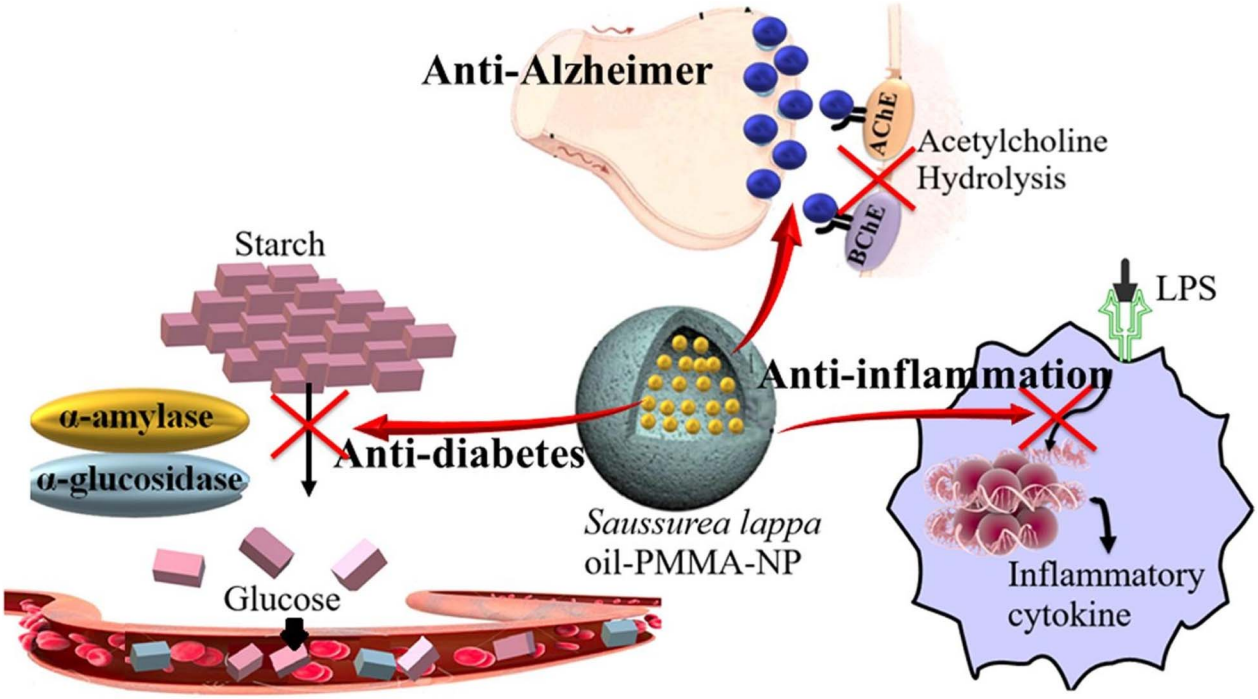

Fig. 7 Therapeutic activities of *S. lappa*-loaded PMMA nanoparticles. The nanoformulation exhibited anti-diabetic activity by inhibiting α-amylase and α-glucosidase enzymes, thereby reducing glucose release. It also demonstrated cholinergic modulation activities, and consequently could delay progression of Alzheimer's disease, by inhibiting AChE and BChE. Additionally, it showed anti-inflammatory action by downregulating LPS-induced expression of pro-inflammatory cytokines. Reproduced with permission.[94] Elsevier, 2021.

increased at day 14 in the *S. costus*-CS group, indicating an early complement response, whereas the free *S. costus* group did not show a sustained time-dependent rise in C3. Importantly, tumor necrosis factor-alpha (TNF-α) was markedly suppressed in *S. costus*-CS NPs-treated rats. Both free *S. costus* extract and *S. costus*-CS NPs reduced TNF-α relative to the immunosuppressed group, but the nanoformulation achieved the most sustained and profound effect. *S. costus*-CS NPs were the only conjugate that significantly reduced TNF-α levels below those of the control group across the entire experimental period and displayed the lowest TNF-α values among all plant-CS nanoformulations, underlining the particularly strong anti-inflammatory potential of the nanoformulated *S. costus* extract compared with its free counterpart. In parallel, histopathological evaluations of the spleen demonstrated a clear reversal of dexamethasone-induced white pulp atrophy and restoration of normal follicular architecture in animals treated with *S. costus*-CS NPs, supported by a pronounced elevation in Ki-67 expression. Notably, the highest Ki-67 area percentage was recorded in both the *S. costus* extract and *S. costus*-CS NPs groups, indicating that nanoencapsulation preserves the intrinsic lymphoproliferative capacity of the traditional extract while enhancing its systemic immunomodulatory and anti-inflammatory profile relative to free *S. costus*. Liver (ALT, AST) and kidney (urea, creatinine) function markers remained within normal ranges, indicating no toxicity. Also, histology of liver and kidney of *S. costus*-CS NPs-treated animals showed normal hepatocyte architecture and no signs of glomerular or tubular damage. Thus, within this comparative study, the *S. costus*-CS nanoformula were superior not only against other plant-based chitosan nanoformulations but also relative to free *S. costus* extract, offering stronger and faster immunomodulatory effects with a comparable safety profile.[91]

Anti-inflammatory, anti-diabetic, and anti-Alzheimer activities of *S. costus* essential oil were evaluated after incorporation in polymethyl methacrylate (PMMA) nanocapsules (Fig. 7).[94] *S. costus* essential oil was extracted by supercritical CO_2 extraction and was rich in dehydrocostus lactone (55.39%) and costunolide (8.87%). Nanoprecipitation was used to prepare *S. costus*-PMMA nanocapsules with a mean size of 145 ± 1 nm, PDI of 0.18 ± 0.01, and zeta potential of +45 ± 2 mV. TEM images indicated spherical morphology, while FTIR confirmed successful encapsulation of the essential oil. Cytotoxicity was assessed on human lung epithelial (A549) cells using the LDH assay. *S. costus*-PMMA nanocapsules were non-cytotoxic at 12.5–25 μg mL^{-1}, similar to free *S. costus* essential oil, although the encapsulated form became more cytotoxic at higher concentrations (≥50 μg mL^{-1}), consistent with increased cellular uptake and bioavailability upon nanoencapsulation. Anti-inflammatory effects were investigated in LPS-stimulated A549 cells using qRT-PCR and gelatin zymography. *S. costus*-PMMA nanocapsules significantly reduced the expression of TNF-α, IL-1β and GM-CSF and suppressed MMP-9 activity, whereas blank PMMA nanoparticles showed no such effect, confirming that the anti-inflammatory activity arised from the *S. costus* oil and is potentiated by its nano-encapsulation.

Cholinesterase inhibition assays revealed that encapsulation markedly enhanced the anti-Alzheimer potential of *S. costus*.

The IC_{50} values against AChE (Acetylcholinesterase) decreased from 67.4 ± 3.7 μg mL^{-1} for free oil to 25.0 ± 2.0 μg mL^{-1} for *S. costus*-PMMA, and against BChE (butyrylcholinesterase) from 17.4 ± 1.1 μg mL^{-1} to 14.9 ± 1.9 μg mL^{-1}, while both nano-formulated and free oil compared favorably with galantamine for BChE inhibition. This improvement is attributed to the α-methylene-γ-butyrolactone moiety of sesquiterpene lactones, which interacts with sulfhydryl groups on cholinesterases.

Inhibition of carbohydrate-digesting enzymes (α-amylase and α-glucosidase) was also evaluated to assess antidiabetic activity. For α-amylase, nanoencapsulation substantially increased potency, with IC_{50} decreasing from 65.9 ± 1.7 μg mL^{-1} (free *S. costus* oil) to 22.9 ± 0.3 μg mL^{-1} (*S. costus*-PMMA), both outperforming acarbose (365.3 ± 10.7 μg mL^{-1}). For α-glucosidase, the free oil remained more potent (IC_{50} 42.1 ± 3.0 μg mL^{-1}) than the encapsulated form (75.8 ± 4.4 μg mL^{-1}), an effect attributed to the slower release of the oil from the PMMA matrix. Nevertheless, both free and nanoencapsulated *S. costus* outperformed acarbose (271.7 ± 7.1 μg mL^{-1}).

Thus, encapsulation of *S. costus* essential oil in PMMA enhanced its solubility, stability, cellular uptake and sustained release, resulting in stronger anti-inflammatory, anti-cholinesterase and α-amylase inhibitory activities than the traditional free extract, while maintaining superior safety at non-cytotoxic concentrations.[94]

Moelyanto *et al.* evaluated whether *S. costus*-loaded Eudragit® RS100 polymeric nanoparticles can attenuate *Porphyromonas gingivalis*-induced periodontal inflammation by quantifying changes in NF-κB and TNF-α at 2 and 5 days post-treatment, addressing the need for bioavailable, plant-based anti-inflammatories in periodontitis.[95] For this purpose, the nanoparticles were prepared using the nanoprecipitation method, having a mean size of 119.7 nm with PDI of 0.182. For biological testing (*in vivo*), male Wistar rats received *P. gingivalis* injections into the mandibular gingival sulcus every 3 days for 14 days until periodontitis was evident. Treated groups were dosed with the prepared *S. costus*-loaded nanoparticles once daily. The inflammatory signaling in alveolar bone was evaluated for NF-κB p65 (transcription factor that drives the expression of pro-inflammatory cytokines) and TNF-α (promotes inflammation, osteoclast activity, and alveolar bone resorption). Results have shown a significant reduction in the expression of both NF-κB ($p = 0.001$) and TNF-α ($p = 0.002$) by day 5 in the alveolar bone of the lower, indicating effective suppression of the periodontal inflammatory cascade. Furthermore, rats exhibited gingival redness, edema, recession, and bleeding on probing, and radiographs showed decreased bone density with

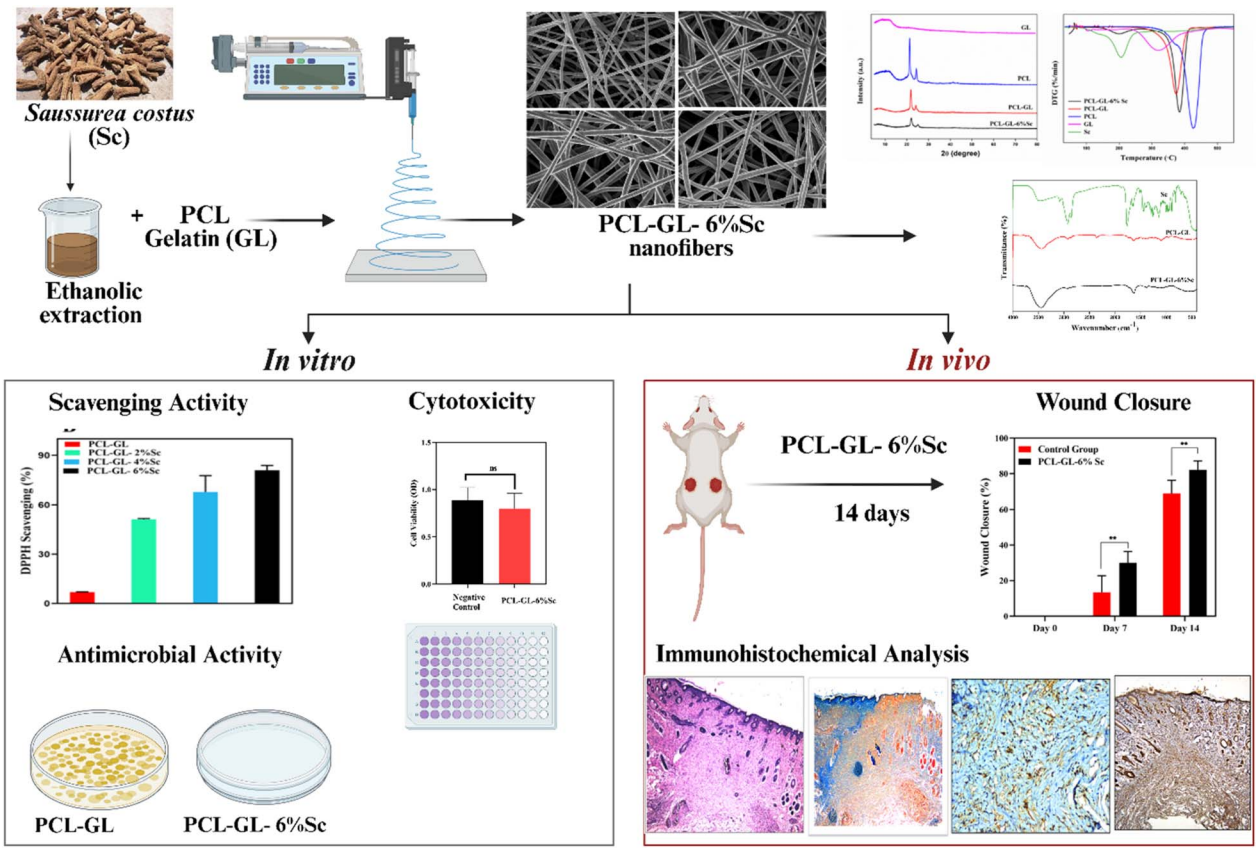

Fig. 8 Evaluation of *S. costus*-loaded PCL–GL nanofibers for wound healing applications. Nanofibers were characterized using SEM, FTIR, XRD, and TGA to confirm successful nanofiber formation and incorporation of extract phytochemicals. *In vitro* studies demonstrated strong antioxidant (DPPH scavenging) and antimicrobial activities and non-cytotoxic properties. *In vivo* studies showed significantly enhanced rat wound closure and re-epithelialization compared to the untreated control.[96] Copyright license CC BY 3.0.

radiolucent areas around the mandibular central incisors. Histology (H&E) demonstrated chronic inflammatory infiltrates composed of lymphocytes, plasma cells, and macrophages in the alveolar bone, together confirming active periodontitis prior to treatment.[95]

7.2.2 Electrospun nanofibers. Lababidi *et al.* synthesized polycaprolactone–gelatin (PCL–GL) nanofibers loaded with 6% ethanolic extract of *S. costus* (*S. costus* -loaded PCL–GL) and assessed their antimicrobial, antioxidant, anti-inflammatory, and wound healing potency (Fig. 8).[96] Incorporation of the *S. costus* extract increased the nanofiber diameter to 253.07 ± 44.54 nm (SEM). Fast Fourier transform (FFT) confirmed the alignment of *S. costus* -loaded PCL–GL. FTIR analysis indicated bonding interactions, XRD confirmed crystallinity of PCL, and thermal stability was evaluated by TGA. Water contact angle was 54.6° ± 2.03, indicating enhanced hydrophilicity upon incorporation of *S. costus* into the nanofibers. The *in vitro* release profile of *S. costus* from nanofibers demonstrated a controlled, triphasic release behavior over 7 days. An initial burst release occurred during the first 12 hours, attributed to extract located near or on the fiber surface, with release value of 36.72%. This was followed by a slower, controlled diffusion phase, likely associated with gradual polymer swelling and limited matrix degradation, with cumulative release after 72 hours reaching 43.33 by day 7, the final bulk erosion phase was observed, achieving cumulative release value of 45.99%. Release kinetic modeling showed that the data best fitted the Higuchi model, indicating diffusion-controlled release through the polymer matrix. The addition of hydrophilic GL facilitated swelling and pore formation, enhancing extract diffusion compared to PCL alone. The Korsmeyer–Peppas release exponent further confirmed Fickian diffusion as the predominant release mechanism.[96] Antimicrobial activity of *S. costus* -loaded PCL–GL against *P. aeruginosa*, *S. aureus*, and *E. coli* achieved a log reduction of 7 (99.999% inhibition) in all strains. Antioxidant activity (DPPH assay) was 80.85%. MTT assay demonstrated biocompatibility with no significant cytotoxic effects on human skin fibroblasts. *In vivo* studies using male albino rats revealed that *S. costus* -loaded PCL–GL-treated wounds induced significant closure of the wound (82.22 ± 4.96%) *vs.* untreated wounds (68.88 ± 7.37%). Additionally, total leukocyte count and inflammatory markers were downregulated, while pro-apoptotic and angiogenic genes were upregulated. Histological and immunohistochemical analysis confirmed thick epithelial regeneration, dense collagen deposition, moderate VEGF and TGF-β1 expression, and high BAX levels in treated wounds. The findings suggest that *S. costus* -loaded PCL–GL nanofibers represent a safe intervention to accelerate wound healing.[96]

7.2.3 Lipid-based nanoparticles. Alamoudi *et al.* encapsulated costunolide (a major sesquiterpene lactone occurring predominantly in *S. costus*) into bilosome nanoparticles to overcome its poor solubility and permeability and thereby boost its anti-colon-cancer activity against LS174T colorectal adenocarcinoma cells.[97] Costunolide-loaded bilosomes were prepared by thin film hydration using cholesterol, Span-85 and bile salt. Higher cholesterol : Span ratios and bile salt levels increased EE%, with the optimum condition (cholesterol : Span 1 : 5 and bile salt 0.5 mM) yielding a vesicle size of 119.7 ± 3.63 nm and an entrapment efficiency of 63.4 ± 3.59%, indicating efficient drug loading in a nanoscale carrier. *In vitro* cytotoxicity quantified by the sulforhodamine B assay (48 h) showed that costunolide-loaded bilosomes (IC_{50} = 6.20 μM) were more than twice as potent as free costunolide (IC_{50} = 15.78 μM) against LS174T cells, while oxaliplatin (positive control) had an IC_{50} of 0.70 μM and the blank bilosomes were much less toxic (IC_{50} = 50.08 μM). Selectivity was further supported in normal human colonic epithelial cells (HCoEp), where IC_{50} values were 65.11 μM for blank bilosomes, 55.75 μM for free costunolide, and 25.84 μM for costunolide-loaded bilosomes, indicating that nanoencapsulation preferentially enhances cytotoxicity in cancer cells while maintaining an acceptable safety margin in normal cells. Cell-cycle analysis revealed that both free costunolide and loaded-bilosomes increased the sub-G1 population, consistent with apoptotic DNA fragmentation, but the nanoformulation caused a more pronounced sub-G1 accumulation. Annexin-V/PI staining confirmed a stronger pro-apoptotic effect for costunolide-loaded bilosomes, with a 208% increase in late apoptosis *vs.* control and higher necrosis (+144.7% *vs.* control and +42.6% *vs.* free costunolide), showing that the nanoformulation drives programmed cell death more effectively than the free compound. Costunolide-loaded bilosomes induced greater up-regulation of CASP3, BAX and TP53 and more pronounced down-regulation of BCL2 compared with free costunolide, accompanied by a 173.2% increase in ROS *vs.* control (97.0% *vs.* free costunolide), loss of mitochondrial membrane potential and cytochrome-c release, indicating more efficient activation of the intrinsic mitochondrial apoptotic pathway. Therefore, bilosomal encapsulation of this *S. lappa*-derived component significantly enhanced its cytotoxic, pro-apoptotic and mitochondrial ROS-mediated effects relative to traditional (non-encapsulated) costunolide, while preserving selectivity toward malignant over normal colonic epithelial cells.[97]

7.2.4 Inorganic nanoparticles. Niu *et al.* enhanced the aqueous solubility and gastric instability of costunolide, a key *S. costus* sesquiterpene lactone, by loading it into pH-responsive mesoporous silica nanoparticles coated with a methacrylic acid copolymer (Eudragit/MAC) to improve its dissolution in intestinal fluid and anti-liver-fibrosis efficacy.[98] The nanoparticles were synthesized using cetyltrimethylammonium bromide (CTAB) as a template, then costunolide was adsorptively loaded into the mesopores and finally MAC-coated. TEM imaging showed 10 nm channels in empty mesoporous silica nanoparticles that became less distinct after loading and coating, and N_2 sorption revealed marked decreases in surface area and pore volume, together confirming pore filling and encapsulation of costunolide. HPLC quantified drug loading at 30.5 ± 2.45%. The release of costunolide was evaluated in simulated stomach (pH 1.0) *versus* intestinal (pH 6.8) fluid. In acidic medium (pH 1.0), pure costunolide was highly unstable, with its remaining content dropping to 1.68% ± 0.47% within 2 h. In contrast, the coated nanoparticles released only a small initial surface fraction detectable within the first 10 min, after which costunolide became hardly detectable beyond 30 min, indicating that the MAC coating effectively acted as an acid

shield and prevented further drug release and degradation. Under intestinal conditions (pH 6.8), both loaded and coated + loaded nanoparticles showed rapid and almost complete release within 45 min, whereas only 12.8% ± 2.39% of pure costunolide dissolved over the same period. Thus, MAC-coating protected costunolide in the stomach and then enabled fast release in the intestine, improving both its stability and dissolution profile for absorption.[98] In human hepatic stellate cells (LX-2), blank nanoparticles were biocompatible, and at an equal nominal dose, loaded + coated nanoparticles suppressed fibrogenic proteins (TGF-β1, MMP2, α-SMA, COL1A1) more strongly than free costunolide dispersed in water, indicating that improved dispersion and release translate into a stronger cellular antifibrotic response. Crucially, this superiority was confirmed *in vivo* in a bile duct ligation rat model. Loaded nanoparticles administered at half the costunolide dose produced greater antifibrotic benefit than free costunolide, with lower necrosis scores, smaller Sirius Red-positive collagen areas, more pronounced reductions in hepatic TGF-β1, MMP2 and α-SMA, and significant improvements in serum ALT/AST, whereas free costunolide produced weaker or limited changes. Therefore, these findings provide a clear comparison showing that, compared with traditional (non-encapsulated) costunolide, the nanoformulated *S. costus* constituent exhibits superior gastric stability, intestinal dissolution, antifibrotic potency and dose-sparing efficacy in preclinical models.[98]

8. Discussion

The studies summarized in this review collectively demonstrate that nanoformulations enhance the therapeutic potential of *S. costus* extracts. Across different platforms, nanoencapsulation was shown to improve solubility, protect labile sesquiterpene lactones and essential oils from degradation, and increase cellular uptake, often leading to stronger biological effects than those observed with the corresponding free extracts or pure compounds.[89–98] Furthermore, these nanoformulations achieved comparable or superior activity to conventional therapies, positioning *S. costus* as a promising candidate for plant-based nanotherapeutics rather than simply a traditional herbal remedy.[90–99,101] Chitosan-based systems and polymeric nanocapsules amplify immunomodulatory, anti-inflammatory, antidiabetic and anti-Alzheimer activities, and in some cases reduce the effective dose required to achieve a therapeutic response.[89,91,94] For example, chitosan nanoparticles and PMMA nanocapsules improved complement activation, TNF-α suppression, cholinesterase inhibition and α-amylase inhibition relative to free extract or essential oil, while maintaining acceptable biocompatibility in the tested models.[91,94] Similarly, lipid-based bilosomes and pH-responsive inorganic carriers such as mesoporous silica coated with methacrylic copolymers illustrate how rational design can overcome the poor solubility and gastric instability of costunolide, resulting in enhanced antifibrotic or anticancer activity and dose-sparing effects *in vivo*.[97,98] These trends support that nanocarriers can be tailored to address specific biopharmaceutical limitations of *S. costus* and its constituents, thereby unlocking pharmacological effects that are not fully accessible with traditional formulations.[91,94,97,98]

Topical and localized delivery systems represent another promising area for *S. costus* nanoformulations. Silver nanoparticles embedded in chitosan hydrogels, as well as *S. costus*-loaded PCL–GL electrospun nanofibers, have shown robust antibacterial, antioxidant and wound-healing properties *in vitro* and *in vivo*.[96,99] These platforms combine the intrinsic antimicrobial and anti-inflammatory properties of *S. costus* with the structural benefits of hydrogels or fibrous scaffolds, such as moisture retention, controlled release and physical support for tissue regeneration.[96,99] The demonstration of accelerated wound closure and improved collagen deposition suggests that *S. costus* nanomaterials could be used for cutaneous and mucosal indications where localized high concentrations (while minimizing systemic exposure) are desired.[96,99]

Metal and metal oxide nanoparticles synthesized using *S. costus* extracts (Ag, Cu, ZnO, MgO, Pd, IONPs, CuO) also show impressive antimicrobial and, in some cases, anticancer activities, reflecting synergistic effects between the metallic core and phytochemical capping layers.[90,92,93,99–104,107,108] These systems have very high reactivity and strong ROS-generating capacity underlining the need for careful balance between therapeutic benefit and potential toxicity, especially for systemic applications.[92,93,98,100,106–108,110–112] Polymeric and lipid/inorganic carriers appear particularly suitable for systemic delivery and for overcoming solubility and stability barriers,[89,91,94,95,97,98] whereas hydrogels and nanofibers are more appropriate for topical wound management,[96,99] and metal/metal oxide nanoparticles may be most useful when high local antimicrobial activity is required.[90,92,93,99–104,107,108] This review aims to highlight the use of nanoformulations to maximize the value of *S. costus* as a medicinal plant and to identify biomedical applications where further preclinical and translational work are needed.

9. Challenges and limitations

Despite the reported biomedical application of *S. costus* nanoformulations, several challenges still need to be addressed. As for all plant extracts, differences in geographical origin and cultivation conditions cause batch variability in phytochemical composition of *S. costus* extract. In addition to yield percent variability and low stability of the extract, different extraction methods could also yield variable sets of phytochemicals. The reported chemical components in *S. costus* extracts fluctuate dramatically as reported by different studies, making it difficult to establish a reproducible therapeutic profile across different batches.[74]

EE% values were generally in the range of 50–65%, a pattern that is consistent with the pronounced hydrophobicity of major *S. costus* constituents, such as sesquiterpene lactones and essential oils.[89,91,98] However, several studies did not report encapsulation parameters, EE% and loading capacity, making it difficult to assess incorporation efficiency or compare systems quantitatively. The key variables that are known to influence EE%, including carrier composition, medium pH, solvent removal conditions and nanoparticle size, were rarely

explored.[113] Lack of these parameters limits cross-study comparability to optimize *S. costus*-loaded nanoformulations for future therapeutic applications.

Although nanoencapsulation of *S. costus* compounds could protect them from light and thermal degradation, long-term stability studies are still needed.[92] To date, most published work on *S. costus*-based nanoformulations consists of *in vitro* experiments or short-term *in vivo* studies. For the majority of nanosystems, available data are limited to physicochemical characterization and *in vitro* cytotoxicity/efficacy assays, with no pharmacokinetic analysis and only very limited, non-comprehensive *in vivo* toxicity profiling. There is, therefore, a clear need for long-term animal studies and clinical validation to define the therapeutic efficacy, pharmacodynamics and pharmacokinetics of nanoformulated *S. costus* extracts in humans. In addition, metal-based *S. costus* nanosystems raise specific safety and cytotoxicity concerns that are still insufficiently addressed.[110] Most studies on silver, zinc oxide and other metal nanoparticles synthesized using *S. costus* extracts focused on antimicrobial or anticancer efficacy, while providing little or no information on systemic toxicity, hemocompatibility, genotoxicity, biodistribution, or elimination pathways.[92,93,99,106] Metal nanoparticles can generate reactive oxygen species, induce oxidative stress, interact with cellular membranes and proteins, and potentially accumulate in clearance organs such as the liver, spleen, and kidneys, particularly at higher doses or upon repeated administration.[111,112] *In vitro* work has indicated dose-dependent cytotoxicity and intracellular accumulation in mammalian cells for some *S. costus*-based formulations, but comprehensive dose–response and long-term toxicity studies are lacking.[92,93,99,106] Consequently, careful toxicological evaluation and dose optimization are required before metal-based *S. costus* nanosystems can be considered for translational or clinical use.[92,114] The available studies evaluating *S. costus*-based nanoformulations are still limited, and future research should prioritize systematic comparative studies in which *S. costus* nanoformulations are assessed alongside other medicinal plants. Such comparative work will be essential to clarify whether *S. costus* provides consistent advantages over other botanicals in terms of efficacy, safety and translational potential. Finally, large-scale production of these nanoformulations should be explored to address technical challenges, develop relevant quality control procedures, and meet regulatory guidelines.

The studies summarized in this review collectively demonstrate that nanoformulations enhance the therapeutic potential of *S. costus* extracts. Across different platforms, nanoencapsulation was shown to improve solubility, protect labile sesquiterpene lactones and essential oils from degradation, and increase cellular uptake, often leading to stronger biological effects than those observed with the corresponding free extracts or pure compounds.[89–98] Furthermore, these nanoformulations achieved comparable or superior activity to conventional therapies, positioning *S. costus* as a promising candidate for plant-based nanotherapeutics rather than simply a traditional herbal remedy.[90–99,101] Chitosan-based systems and polymeric nanocapsules amplify immunomodulatory, anti-inflammatory, antidiabetic and anti-Alzheimer activities, and in some cases reduce the effective dose required to achieve a therapeutic response.[89,91,94] For example, chitosan nanoparticles and PMMA nanocapsules improved complement activation, TNF-α suppression, cholinesterase inhibition and α-amylase inhibition relative to free extract or essential oil, while maintaining acceptable biocompatibility in the tested models.[91,94] Similarly, lipid-based bilosomes and pH-responsive inorganic carriers such as mesoporous silica coated with methacrylic copolymers illustrate how rational design can overcome the poor solubility and gastric instability of costunolide, resulting in enhanced antifibrotic or anticancer activity and dose-sparing effects *in vivo*.[97,98] These trends support that nanocarriers can be tailored to address specific biopharmaceutical limitations of *S. costus* and its constituents, thereby unlocking pharmacological effects that are not fully accessible with traditional formulations.[91,94,97,98]

Topical and localized delivery systems represent another promising area for *S. costus* nanoformulations. Silver nanoparticles embedded in chitosan hydrogels, as well as *S. costus*-loaded PCL–GL electrospun nanofibers, have shown robust antibacterial, antioxidant and wound-healing properties *in vitro* and *in vivo*.[96,99] These platforms combine the intrinsic antimicrobial and anti-inflammatory properties of *S. costus* with the structural benefits of hydrogels or fibrous scaffolds, such as moisture retention, controlled release and physical support for tissue regeneration.[96,99] The demonstration of accelerated wound closure and improved collagen deposition suggests that *S. costus* nanomaterials could be used for cutaneous and mucosal indications where localized high concentrations (while minimizing systemic exposure) are desired.[96,99]

10. Conclusions

S. costus has been known for decades for its therapeutic uses in multiple cultures including traditional Ayurveda, Chinese, and Tibetan medicine. It has been used in treating a broad spectrum of medical conditions such as respiratory, digestive, gynecological, and infectious diseases. The remarkable biological activities of *S costus* are attributed to its rich content of pharmacologically active phytochemicals including sesquiterpene lactones, costunolide, flavonoids, phenolics, and essential oils. However, the full potential of this medicinal plant remains largely untapped in clinical settings due to its low water solubility and bioavailability, lack of targetability, and environmental instability. Incorporation of *S. costus*-derived compounds into metallic nanoparticles, polymeric, lipid-based, inorganic nanocarriers and electrospun nanofibers was introduced to overcome these limitations. These nanoformulations were reported to exert significant antimicrobial, anticancer, antioxidant, anti-inflammatory, and wound healing activities. Additional nanoformulations would help transform *S. costus* from traditional medicine into a modern, evidence-based therapeutic for diverse biomedical applications.

Conflicts of interest

The authors declare no potential competing interests.

Data availability

No primary research results, software or code have been included and no new data were generated or analysed as part of this review.

Acknowledgements

The current work was funded by a grant from the American University in Cairo to Prof. Hassan Azzazy.

References

1 J. Kumar and M. Pundir, Phytochemistry and pharmacology of Saussurea genus (Saussurea lappa, Saussurea costus, Saussurea obvallata, Saussurea involucrata), *Mater. Today: Proc.*, 2022, **56**, 1173–1181, DOI: 10.1016/j.matpr.2021.11.145.

2 H. He, T. Wang, C. Tang, Z. Cao, X. Pu, Y. Li and X. Li, Complete Chloroplast Genomes of Saussurea katochaete, Saussurea superba, and Saussurea stella: Genome Structures and Comparative and Phylogenetic Analyses, *Genes*, 2023, **14**(11), 2002, DOI: 10.3390/genes14112002.

3 N. Nyamgerel, S. Baasanmunkh, B. Oyuntsetseg, Z. Tsegmed, G.-A. Bayarmaa, G. Lazkov, E. Pyak, H.-Y. Gil, I. Park and H. J. Choi, Comparative plastome analysis and taxonomic classification of snow lotus species (Saussurea, Asteraceae) in Central Asia and Southern Siberia, *Funct. Integr. Genomics*, 2024, **24**(2), 42, DOI: 10.1007/s10142-024-01309-y.

4 J. S. Butola and S. S. Samant, Saussurea species in Indian Himalayan Region: diversity, distribution and indigenous uses, *Int. J. Plant Biol.*, 2010, **1**(1), e9, DOI: 10.4081/pb.2010.e9.

5 X. Zhang, Y. Sun, J. B. Landis, J. Shen, H. Zhang, T. Kuang, W. Sun, J. Sun, B. B. Tiamiyu, T. Deng, *et al.*, Transcriptomes of Saussurea (Asteraceae) Provide Insights into High-Altitude Adaptation, *Plants*, 2021, **10**(8), 1715.

6 X. Zhang, T. Deng, M. J. Moore, Y. Ji, N. Lin, H. Zhang, A. Meng, H. Wang, Y. Sun and H. Sun, Plastome phylogenomics of Saussurea (Asteraceae: Cardueae), *BMC Plant Biol.*, 2019, **19**(1), 290, DOI: 10.1186/s12870-019-1896-6.

7 T. Yi, Z.-Z. Zhao, Z.-L. Yu and H.-B. Chen, Comparison of the anti-inflammatory and anti-nociceptive effects of three medicinal plants known as "Snow Lotus" herb in traditional Uighur and Tibetan medicines, *J. Ethnopharmacol.*, 2010, **128**(2), 405–411, DOI: 10.1016/j.jep.2010.01.037.

8 D. P. Jani and K. D. Jani, Analytical profile of Kushtha (Saussurea lappa) extensively used medicinal plant in Ayurveda system of medicine, *J. Aayurveda Integr. Med. Sci.*, 2017, **2**(04), 63–67, DOI: 10.21760/jaims.v2i04.241.

9 S. Yun and S.-C. Kim, Comparative plastomes and phylogenetic analysis of seven Korean endemic Saussurea (Asteraceae), *BMC Plant Biol.*, 2022, **22**(1), 550, DOI: 10.1186/s12870-022-03946-6.

10 K. Jatoth, P. K. Anoor, R. Kande and S. Burgula, Saussurea gossypiphora extracts reduce inflammation by reversing inflammatory cytokine levels in in-vitro and in-vivo, *Phytomed. Plus*, 2025, **5**(1), 100709, DOI: 10.1016/j.phyplu.2024.100709.

11 W.-L. Pang, T.-G. Li, Y.-Y. Wang, L.-Y. Song, L. Li, X.-Y. Li, Y. Qiu and Z.-S. Yang, Saussurea costus alleviates ulcerative colitis by regulating the gut microbiota and improving intestinal barrier integrity, *Front. Cell. Infect. Microbiol.*, 2025, **15**, 1528578, DOI: 10.3389/fcimb.2025.1528578.

12 N. G. M. Attallah, A. Kabbash, W. A. Negm, E. Elekhnawy, R. Binsuwaidan, O. M. Al-Fakhrany, M. A. Shaldam, E. Moglad, M. Tarek, N. Samir, *et al.*, Protective Potential of Saussurea costus (Falc.) Lipsch. Roots against Cyclophosphamide-Induced Pulmonary Injury in Rats and Its In Vitro Antiviral Effect, *Pharmaceuticals*, 2023, **16**(2), 318, DOI: 10.3390/ph16020318.

13 A. A. Fitrianingsih, D. Santosaningsih, S. Djajalaksana, R. Mutiah, M. I. Lusida, S. S. Karyono and S. R. Prawiro, Network pharmacology and in silico investigation on Saussurea lappa for viral respiratory diseases, *Trop. J. Nat. Prod. Res.*, 2024, **8**(1), 5889–5896.

14 A. Saklani, B. Hegde, P. Mishra, R. Singh, M. Mendon, D. Chakrabarty, D. V. Kamath, A. Lobo, P. D. Mishra, N. M. Dagia, *et al.*, NF-κB dependent anti-inflammatory activity of chlorojanerin isolated from Saussurea heteromalla, *Phytomedicine*, 2012, **19**(11), 988–997, DOI: 10.1016/j.phymed.2012.05.016.

15 Z. Niktabe, T. Eftekhaar, M. Mirabzadeh Ardakani, M. S. Yekaninejad, L. Shirbeigi, N. Ebadi, N. Masoudi and S. Bagheri, Efficacy of Saussurea costus (qost) oil as an Iranian traditional medicine product on female urinary incontinence; double blinded randomized clinical trial, *Res. J. Pharmacogn.*, 2018, **5**(3), 47–55, DOI: 10.22127/rjp.2018.64876.

16 H. Idriss, B. Siddig, P. González-Maldonado, H. Elkhair, A. I. Alakhras, E. M. Abdallah, A. O. Elzupir and P. H. Sotelo, Inhibitory activity of Saussurea costus extract against bacteria, candida, herpes, and SARS-CoV-2, *Plants*, 2023, **12**(3), 460, DOI: 10.3390/plants12030460.

17 M. M. Pandey, S. Rastogi and A. K. S. Rawat, Saussurea costus: Botanical, chemical and pharmacological review of an ayurvedic medicinal plant, *J. Ethnopharmacol.*, 2007, **110**(3), 379–390, DOI: 10.1016/j.jep.2006.12.033.

18 S. I. Ali and V. Venkatesalu, Botany, traditional uses, phytochemistry and pharmacological properties of Saussurea costus – An endangered plant from Himalaya-A review, *Phytochem. Lett.*, 2022, **47**, 140–155, DOI: 10.1016/j.phytol.2021.12.008.

19 K. Rautela, Y. Bisht, A. Kumar, A. Sharma and A. K. Jugran, Diverse Ecological and Biological Roles of Secondary Metabolites of Saussurea costus (Falc.) Lipsch, in *Plant Specialized Metabolites: Phytochemistry, Ecology and Biotechnology*, Springer, 2023, pp. 1–29.

20 R. Semwal, K. Joshi, A. Pandian, P. Badoni and D. Semwal, Biological applications and secondary metabolites of

Saussurea costus (Falc.) Lipsch, *J. Conv. Knowl. Holist. Health*, 2020, **4**(1), 1–8.

21 H. Jain and N. Chella, Solubility Enhancement Techniques for Natural Product Delivery, in *Sustainable Agriculture Reviews 43: Pharmaceutical Technology for Natural Products Delivery Vol. 1 Fundamentals and Applications*, ed. A. Saneja, A. K. Panda and E. Lichtfouse, Springer International Publishing, 2020, pp. 33–66.

22 M. Abhinav, J. Neha, G. Anne and V. Bharti, Role of novel drug delivery systems in bioavailability enhancement: At a glance, *Int. J. Drug Deliv. Technol.*, 2016, **6**(1), 7–26.

23 H. Chopra, S. Sharma, S. Yousaf, R. Naseer, S. Ahmed and A. A. Baig, Applications of nanotechnology-based approaches for targeted delivery of nutraceuticals, in *Handbook of Nanotechnology in Nutraceuticals*, CRC Press, 2022, pp. 329–346.

24 P. S. Phansalkar, Z. Zhang, S. Verenich and P. M. Gerk, Pharmacokinetics and Bioavailability Enhancement of Natural Products, in *Natural Products for Cancer Chemoprevention: Single Compounds and Combinations*, ed. J. M. Pezzuto and O. Vang, Springer International Publishing, 2020, pp. 109–141.

25 C. Turek and F. C. Stintzing, Stability of essential oils: a review, *Compr. Rev. Food Sci. Food Saf.*, 2013, **12**(1), 40–53, DOI: 10.1111/1541-4337.12006.

26 C. Turek and F. C. Stintzing, Impact of different storage conditions on the quality of selected essential oils, *Food Res. Int.*, 2012, **46**(1), 341–353, DOI: 10.1016/j.foodres.2011.12.028.

27 C. Qi, G. Liu, Y. Ping, K. Yang, Q. Tan, Y. Zhang, G. Chen, X. Huang and D. Xu, A comprehensive review of nano-delivery system for tea polyphenols: Construction, applications, and challenges, *Food Chem.: X*, 2023, **17**, 100571, DOI: 10.1016/j.fochx.2023.100571.

28 V. P. Chavda, A. B. Patel, K. J. Mistry, S. F. Suthar, Z.-X. Wu, Z.-S. Chen and K. Hou, Nano-drug delivery systems entrapping natural bioactive compounds for cancer: recent progress and future challenges, *Front. Oncol.*, 2022, **12**, 867655, DOI: 10.3389/fonc.2022.867655.

29 Y. Lv, W. Li, W. Liao, H. Jiang, Y. Liu, J. Cao, W. Lu and Y. Feng, Nano-drug delivery systems based on natural products, *Int. J. Nanomed.*, 2024, 541–569, DOI: 10.2147/IJN.S443692.

30 C. Puglia, R. Pignatello, V. Fuochi, P. M. Furneri, M. R. Lauro, D. Santonocito, R. Cortesi and E. Esposito, Lipid nanoparticles and active natural compounds: A perfect combination for pharmaceutical applications, *Curr. Med. Chem.*, 2019, **26**(24), 4681–4696, DOI: 10.2174/0929867326666190614123835.

31 A. Faridi Esfanjani, E. Assadpour and S. M. Jafari, Improving the bioavailability of phenolic compounds by loading them within lipid-based nanocarriers, *Trends Food Sci. Technol.*, 2018, **76**, 56–66, DOI: 10.1016/j.tifs.2018.04.002.

32 M. Elmowafy, K. Shalaby, M. H. Elkomy, O. A. Alsaidan, H. A. M. Gomaa, M. A. Abdelgawad and E. M. Mostafa, Polymeric Nanoparticles for Delivery of Natural Bioactive Agents: Recent Advances and Challenges, *Polymers*, 2023, **15**(5), 1123, DOI: 10.3390/polym15051123.

33 S. B. Adeyemi, A. M. Akere, J. I. Orege, O. Ejeromeghene, O. B. Orege and J. O. Akolade, Polymeric nanoparticles for enhanced delivery and improved bioactivity of essential oils, *Heliyon*, 2023, **9**(6), e16543, DOI: 10.1016/j.heliyon.2023.e16543.

34 E. Alphandéry, Natural Metallic Nanoparticles for Application in Nano-Oncology, *Int. J. Mol. Sci.*, 2020, **21**(12), 4412, DOI: 10.3390/ijms21124412.

35 C. Hano and B. H. Abbasi, Plant-based green synthesis of nanoparticles: production, characterization and applications, *Biomolecules*, 2021, **12**(1), 31, DOI: 10.3390/biom12010031.

36 X. Zhang, T. Deng, M. J. Moore, Y. Ji, N. Lin, H. Zhang, A. Meng, H. Wang, Y. Sun and H. Sun, Plastome phylogenomics of Saussurea (Asteraceae: cardueae), *BMC Plant Biol.*, 2019, **19**, 1–10, DOI: 10.1186/s12870-019-1896-6.

37 L. Xu, Z. Song, T. Li, Z. Jin, B. Zhang, S. Du, S. Liao, X. Zhong and Y. Chen, New insights into the phylogeny and infrageneric taxonomy of Saussurea based on hybrid capture phylogenomics (Hyb-Seq), *Plant Diversity*, 2025, **47**(1), 21–33, DOI: 10.1016/j.pld.2024.10.003.

38 L.-S. Xu, S. Herrando-Moraira, A. Susanna, M. Galbany-Casals and Y.-S. Chen, Phylogeny, origin and dispersal of Saussurea (Asteraceae) based on chloroplast genome data, *Mol. Phylogenet. Evol.*, 2019, **141**, 106613, DOI: 10.1016/j.ympev.2019.106613.

39 C.-L. Wu, L.-F. Lin, H.-C. Hsu, L.-F. Huang, C.-D. Hsiao and M.-L. Chou, Saussurea involucrata (Snow Lotus) ICE1 and ICE2 Orthologues Involved in Regulating Cold Stress Tolerance in Transgenic Arabidopsis, *Int. J. Mol. Sci.*, 2021, **22**(19), 10850, DOI: 10.3390/ijms221910850.

40 R. Jyothi and K. M. Srinivas Murthy, An overview on Saussurea obvallata: A spirituo-scientific plant of India, *J. Drug Deliv. Therapeut.*, 2023, **13**(10), 145–146, DOI: 10.22270/jddt.v13i10.5973.

41 P. Semwal, S. Painuli, D. Tewari, R. W. Bussmann, L. M. S. Palni and A. Thapliyal, Brahma Kamal (Saussurea obvallata (DC.) Edgew.): ethnomedicinal, phytochemical and pharmacological overview of an important Himalayan medicinal plant, *Ethnobot. Res. Appl.*, 2020, **19**(40), 1–15, DOI: 10.32859/era.19.40.1-15.

42 Y.-S. Chen and Q. Yuan, Twenty-six new species of Saussurea (Asteraceae, Cardueae) from the Qinghai-Tibetan Plateau and adjacent regions, *Phytotaxa*, 2015, **213**(3), 159–211, DOI: 10.11646/phytotaxa.213.3.1.

43 L. Hu, T. Lu, X. Wang, J. Wang and W. Shi, Conservation Priorities and Demographic History of Saussurea involucrata in the Tianshan Mountains and Altai Mountains, *Life*, 2023, **13**(11), 2209, DOI: 10.3390/life13112209.

44 Y. Zhang, R. Tang, X. Huang, W. Sun, X. Ma and H. Sun, Saussurea balangshanensis sp. nov. (Asteraceae), from the Hengduan Mountains region, SW China, *Nord. J. Bot.*, 2019, **37**(4), DOI: 10.1111/njb.02078.

45 Y. Yang, C. Körner and H. Sun, The ecological significance of pubescence in Saussurea medusa, a high-elevation Himalayan "woolly plant", *Arctic Antarct. Alpine Res.*, 2008, **40**(1), 250–255, DOI: 10.1657/1523-0430(07-009)[YANG]2.0.CO;2.

46 C. Ganbaatar, I. Hoza, P. Valášek, S. Škrovánková, D. Banzragch and N. Tsevegsuren, Anticancer activity of lignan from the aerial parts of saussurea salicifolia (l.) DC, *Czech J. Food Sci.*, 2009, **27**(10), 256–258, DOI: 10.17221/1097-CJFS.

47 S. Eun-Mi, A. Y. Seon, K. Seung-Chul and I. Hyoung-Tak, Taxonomic entity of Saussurea taquetii (Asteraceae) compared with S. japonica and S. pulchella, *Korean J. Plant Taxon.*, 2021, **51**(4), 378–385, DOI: 10.11110/kjpt.2021.51.4.378.

48 D. V. Yusupovsky and E. A. Pyak, The position of two recently described endemic taxa in the system of the genus Saussurea (Asteraceae), *Acta Biol. Sib.*, 2024, **10**, 1479–1486, DOI: 10.1063/1.5009864.

49 E. Fritz and J. Saukel, Interxylary cork of Saussurea discolor and S. pygmaea (Asteraceae), *Biologia*, 2011, **66**(3), 454–457, DOI: 10.2478/s11756-011-0030-5.

50 A. Mansour, H. Bechlem and A. Labed, Traditional herbal medicines and natural remedies used for prevention and treatment of COVID-19 in Algeria, *J. Mol. Pharma. Sci.*, 2022, **1**(1), 74–91.

51 R. El Boullani, M. Barkaoui, K. Lagram, A. El Finti, N. Kamel, A. El Mousadik, M. A. Serghini and F. Msanda, The use of plants in the traditional treatment of diabetes patients: survey in southern Morocco, *Not. Sci. Biol.*, 2022, **14**(4), 11322, DOI: 10.55779/nsb14411322.

52 W.-I. Chik, L. Zhu, L.-L. Fan, T. Yi, G.-Y. Zhu, X.-J. Gou, Y.-N. Tang, J. Xu, W.-P. Yeung, Z.-Z. Zhao, *et al.*, Saussurea involucrata: A review of the botany, phytochemistry and ethnopharmacology of a rare traditional herbal medicine, *J. Ethnopharmacol.*, 2015, **172**, 44–60, DOI: 10.1016/j.jep.2015.06.033.

53 S. Banerjee, S. Banerjee, S. Bose, A. Das and C. Mitra, Saussurea lappa (Kushta): an Indian spice and its potential health benefits, in *Medicinal Spices and Herbs from India*, ed. S. Banerjee and S. Banerjee, Apple Academic Press, New York, 2024, pp. 345–373, DOI: 10.1201/9781003511694-18.

54 S. K. Mehta, S. Prakash and M. S. Rao, Saussurea costus: a treasure in traditional and modern medicine, *Greenaria*, 2024, vol. 2, p.G-24-0943.

55 S. Ansari, Ethnobotany and pharmacognosy of qust/kut (Saussurea lappa, CB Clarke) with special reference of Unani medicine, *Pharmacogn. Rev.*, 2019, **13**(26), 71–76, DOI: 10.5530/phrev.2019.2.7.

56 H. Wei, L. Yan, W. Feng, G. Ma, Y. Peng, Z. Wang and P. Xiao, Research progress on active ingredients and pharmacologic properties of Saussurea lappa, *J. Asian Nat. Prod. Res.*, 2014, **10**(11), 1045–1053, DOI: 10.7178/cocam.00005.

57 R. K. Nadda, A. Ali, R. C. Goyal, P. K. Khosla and R. Goyal, Aucklandia costus (syn. Saussurea costus): Ethnopharmacology of an endangered medicinal plant of the Himalayan region, *J. Ethnopharmacol.*, 2020, **263**, 113199, DOI: 10.1016/j.jep.2020.113199.

58 A. A. M. Elnour and N. H. Abdurahman, Current and potential future biological uses of *Saussurea costus* (Falc.) Lipsch: A comprehensive review, *Heliyon*, 2024, **10**(18), e37790, DOI: 10.1016/j.heliyon.2024.e37790.

59 Convention on International Trade in Endangered Species of Wild Fauna and Flora (CITES), *Checklist of CITES Species: Saussurea costus*, 2026, https://checklist.cites.org/#/en/search/output_layout=alphabetical&level_of_listing=0&show_synonyms=1&show_author=1&show_english=1&show_spanish=1&show_french=1&scientific_name=saussurea&page=1&per_page=20, accessed 16 January 2026.

60 C. P. Kuniyal, J. T. Heinen, B. S. Negi and J. C. Kaim, Is cultivation of Saussurea costus (Asterales: Asteraceae) sustaining its conservation?, *J. Threat. Taxa*, 2019, **11**(13), 14745–14752, DOI: 10.11609/jott.3581.11.13.14745-14752.

61 Z. A. Al-Zayadi, H. K. Shanan and K. A. Al Salihi, Extraction and evaluation of active ingredients of Saussurea costus roots and determination of its antibacterial activity, *IOP Conf. Ser. Earth Environ. Sci.*, 2023, **1225**, 012058, DOI: 10.1088/1755-1315/1225/1/012058.

62 E. Mohsen, A. H. El-Far, K. Godugu, F. Elsayed, S. A. Mousa and I. Y. Younis, SPME and solvent-based GC–MS metabolite profiling of Egyptian marketed Saussurea costus (Falc.) Lipsch. concerning its anticancer activity, *Phytomed. Plus*, 2022, **2**(1), 100209, DOI: 10.1016/j.phyplu.2021.100209.

63 M. H. Abd El-Razek, I. A. Saleh, S. Abdel-Halim, S. M. Bata, A. F. Essa, T. A. Hussien, A. A. El-Beih, T. A. Mohamed and M. E. F. Hegazy, Secondary Metabolites Generated from Saussurea lappa and Ligusticum sinensis Essential Oils by Microwave-Assisted Hydrodistillation: in Silico Molecular Docking and in Vitro Antibacterial Efficacy, *Chem. Biodiversity*, 2023, **20**(8), e202201249, DOI: 10.1002/cbdv.202201249.

64 H. Y. Ahmed, S. M. Kareem, A. Atef, N. A. Safwat, R. M. Shehata, M. Yosri, M. Youssef, M. M. Baakdah, R. Sami, R. S. Baty, *et al.*, Optimization of Supercritical Carbon Dioxide Extraction of Saussurea costus Oil and Its Antimicrobial, Antioxidant, and Anticancer Activities, *Antioxidants*, 2022, **11**(10), 1960, DOI: 10.3390/antiox11101960.

65 K. Rautela, Y. Bisht, A. Kumar, A. Sharma and A. K. Jugran, Diverse Ecological and Biological Roles of Secondary Metabolites of Saussurea costus (Falc.) Lipsch, in *Plant Specialized Metabolites: Phytochemistry, Ecology and Biotechnology*, ed. J.-M. Mérillon and K. G. Ramawat, Springer Nature Switzerland, 2025, pp. 1–29.

66 M. M. Deabes, A.-E. Fatah, I. Sally, S. H. E. Salem and K. M. Naguib, Antimicrobial activity of bioactive compounds extract from Saussurea costus against food spoilage microorganisms, *Egypt. J. Chem.*, 2021, **64**(6), 2833–2843, DOI: 10.21608/ejchem.2021.69572.3528.

67 R. Kumar, Saussurea costus (Falc.) Lipsch root extract supplementation improves diethylnitrosamine-induced hepatic damage in Albino Wistar rats, *Indian J. Vet. Pathol.*, 2024, **48**(4), 351–363, DOI: 10.5958/0973-970X.2024.00059.7.

68 A. M. Marei, The Therapeutic Effects of Costus (Saussurea Lappa) Against Hypercholesterolemia in Male Albino Rats, *Egypt. J. Zool.*, 2022, **78**(78), 31–40, DOI: 10.21608/ejz.2022.121913.1074.

69 X.-F. Hu, W.-X. Liu, R. Zhang, W. Zhang, C. Wang, M. Chen, R. Shu, X.-Z. Yang and Q. Wang, Essential oil from Saussurea costus inhibits proliferation and migration of Eca109 cells via mitochondrial apoptosis and STAT3 signaling, *Asian Pac. J. Trop. Biomed.*, 2022, **12**(6), 253–261, DOI: 10.4103/2221-1691.345517.

70 D.-H. Choi, J.-Y. Kim, J.-H. An, S.-H. Sung and H.-S. Kong, Effects of Saussurea costus on apoptosis imbalance and inflammation in benign prostatic hyperplasia, *J. Ethnopharmacol.*, 2021, **279**, 114349, DOI: 10.1016/j.jep.2021.114349.

71 H. S. Lim, S. E. Jin, O. S. Kim, H. K. Shin and S. J. Jeong, Alantolactone from Saussurea lappa Exerts Antiinflammatory Effects by Inhibiting Chemokine Production and STAT1 Phosphorylation in TNF-α and IFN-γ-induced in HaCaT cells, *Phytother Res.*, 2015, **29**(7), 1088–1096, DOI: 10.1002/ptr.5354.

72 A. A. Shati, M. A. Alkahtani, M. Y. Alfaifi, S. E. I. Elbehairi, F. G. Elsaid, R. Prasanna and M. A. Mir, Secondary Metabolites of Saussurea costus Leaf Extract Induce Apoptosis in Breast, Liver, and Colon Cancer Cells by Caspase-3-Dependent Intrinsic Pathway, *BioMed Res. Int.*, 2020, **2020**(1), 1608942, DOI: 10.1155/2020/1608942.

73 S. T. Elazab, F. A. Safhi, M. Al-Rasheed, A. T. Y. Kishawy, D. Ibrahim and H. A. El-Emam, Glycyrrhiza glabra and Saussurea costus extracts mitigate arsenic-induced nephrotoxicity via orchestrating Nrf2/HO-1 and NF-κB crosstalk and repressing the expression of HSPs genes and apoptosis in broiler chickens, *Toxin Rev.*, 2025, **44**(2), 211–232, DOI: 10.1080/15569543.2024.2419447.

74 H. Idriss, B. Siddig, P. González-Maldonado, H. M. Elkhair, A. I. Alakhras, E. M. Abdallah, A. O. Elzupir and P. H. Sotelo, Inhibitory Activity of Saussurea costus Extract against Bacteria, Candida, Herpes, and SARS-CoV-2, *Plants*, 2023, **12**(3), 460, DOI: 10.3390/plants12030460.

75 H. A. El Gizawy, A. E. El-Haddad, A. M. Saadeldeen and S. A. Boshra, Tentatively Identified (UPLC/T-TOF–MS/MS) Compounds in the Extract of Saussurea costus Roots Exhibit In Vivo Hepatoprotection via Modulation of HNF-1α, Sirtuin-1, C/ebpα, miRNA-34a and miRNA-223, *Molecules*, 2022, **27**(9), 2802, DOI: 10.3390/molecules27092802.

76 E. Abouelwafa, A. Zaki, O. M. Sabry, R. A. El-Shiekh, G. Caprioli and E. Abdel-Sattar, Unveiling the chemical profiling and remarkable modulation of carbohydrate metabolism by costus root, Dolomiaea costus (Falc.) in streptozotocin (STZ)-induced diabetic rats, *J. Ethnopharmacol.*, 2024, **326**, 117911, DOI: 10.1016/j.jep.2024.117911.

77 M. Abdel-Rahman, M. M. Rezk, O. A. Ahmed-Farid, S. Essam and A. E. Abdel Moneim, Saussurea lappa root extract ameliorates the hazards effect of thorium induced oxidative stress and neuroendocrine alterations in adult male rats, *Environ. Sci. Pollut. Res.*, 2020, **27**(12), 13237–13246, DOI: 10.1007/s11356-020-07917-y.

78 L. Moujir, O. Callies, P. M. C. Sousa, F. Sharopov and A. M. L. Seca, Applications of Sesquiterpene Lactones: A Review of Some Potential Success Cases, *Appl. Sci.*, 2020, **10**(9), 3001, DOI: 10.3390/app10093001.

79 L. Chebil, C. Humeau, J. Anthoni, F. Dehez, J.-M. Engasser and M. Ghoul, Solubility of Flavonoids in Organic Solvents, *J. Chem. Eng. Data*, 2007, **52**(5), 1552–1556, DOI: 10.1021/je7001094.

80 Company, T. G. S, HMDB0036688: Costunolide. Human Metabolome Database, https://hmdb.ca/metabolites/HMDB0036688, accessed 2025 April 15, 2025.

81 J. Ueda, Y. Toda, K. Kato, Y. Kuroda, T. Arai, T. Hasegawa, H. Shigemori, K. Hasegawa, J. Kitagawa, K. Miyamoto, *et al.*, Identification of dehydrocostus lactone and 4-hydroxy-β-thujone as auxin polar transport inhibitors, *Acta Physiol. Plant.*, 2013, **35**(7), 2251–2258, DOI: 10.1007/s11738-013-1261-6.

82 P. R. Vadaparthi, K. Kumar, V. U. M. Sarma, Q. A. Hussain and K. S. Babu, Estimation of costunolide and dehydrocostus lactone in Saussurea lappa and its polyherbal formulations followed by their stability studies using HPLC-DAD, *Pharmacogn. Mag.*, 2015, **11**(41), 180, DOI: 10.4103/0973-1296.149736.

83 J. Deng, H. Yang, E. Capanoglu, H. Cao and J. Xiao, 9 – Technological aspects and stability of polyphenols, in *Polyphenols: Properties, Recovery, and Applications*, ed. C. M. Galanakis, Woodhead Publishing, 2018, pp. 295–323.

84 S. S. Kiralan, S. G. Karagoz, G. Ozkan, M. Kiralan and O. Ketenoglu, Changes in Volatile Compounds of Virgin Olive Oil Flavored with Essential Oils During Thermal and Photo-Oxidation, *Food Anal. Methods*, 2021, **14**(5), 883–896, DOI: 10.1007/s12161-020-01926-w.

85 Z. Peng, Y. Wang, X. Gu, X. Guo and C. Yan, Study on the pharmacokinetics and metabolism of costunolide and dehydrocostus lactone in rats by HPLC-UV and UPLC-Q-TOF/MS, *Biomed. Chromatogr.*, 2014, **28**(10), 1325–1334, DOI: 10.1002/bmc.3167.

86 A. Cheminat, J. Stampf, C. Benezra, M. Farrall and J. Frechet, Allergic contact dermatitis to costus: removal of haptens with polymers, *Acta Derm. Venereol.*, 1981, **61**(6), 525–529.

87 L. Oliveira da Silva, M. R. Assunção Ferreira and L. A. Lira Soares, Nanotechnology Formulations Designed with Herbal Extracts and Their Therapeutic Applications–A Review, *Chem. Biodiversity*, 2023, **20**(8), e202201241, DOI: 10.1002/cbdv.202201241.

88 European Medicines Agency, *Final Guideline on Quality of Herbal Medicinal Products/Traditional Herbal Medicinal Products (Revision 3)*, Amsterdam, Netherlands, 2021,

https://www.ema.europa.eu/en/documents/scientific-guideline/final-guideline-quality-herbal-medicinal-productstraditional-herbal-medicinal-products-revision-3_en.pdf.

89 F. A. Alshubaily, Enhanced antimycotic activity of nanoconjugates from fungal chitosan and Saussurea costus extract against resistant pathogenic Candida strains, *Int. J. Biol. Macromol.*, 2019, **141**, 499–503, DOI: 10.1016/j.ijbiomac.2019.09.022.

90 N. S. Al-Radadi, Saussurea costus for sustainable and eco-friendly synthesis of palladium nanoparticles and their biological activities, *Arab. J. Chem.*, 2022, **15**(11), 104294, DOI: 10.1016/j.arabjc.2022.104294.

91 S. S. Milad, S. E. Ali, M. Z. Attia, M. S. Khattab, E. S. El-Ashaal, H. A. Elshoky and A. M. Azouz, Enhanced immune responses in dexamethasone immunosuppressed male rats supplemented with herbal extracts, chitosan nanoparticles, and their conjugates, *Int. J. Biol. Macromol.*, 2023, **250**, 126170, DOI: 10.1016/j.ijbiomac.2023.126170.

92 M. A. Almayouf, R. Charguia, M. A. Awad, A. Ben Bacha and I. Ben Abdelmalek, Nanotherapy for Cancer and Biological Activities of Green Synthesized AgNPs Using Aqueous Saussurea costus Leaves and Roots Extracts, *Pharmaceuticals*, 2024, **17**(10), 1371, DOI: 10.3390/ph17101371.

93 M. Amina, N. M. Al Musayeib, N. A. Alarfaj, M. F. El-Tohamy, H. F. Oraby, G. A. Al Hamoud, S. I. Bukhari and N. M. Moubayed, Biogenic green synthesis of MgO nanoparticles using Saussurea costus biomasses for a comprehensive detection of their antimicrobial, cytotoxicity against MCF-7 breast cancer cells and photocatalysis potentials, *PLoS One*, 2020, **15**(8), e0237567, DOI: 10.1371/journal.pone.0237567.

94 N. Lammari, T. Demautis, O. Louaer, A. H. Meniai, H. Casabianca, C. Bensouici, G. Devouassoux, H. Fessi, A. Bentaher and A. Elaissari, Nanocapsules containing Saussurea lappa essential oil: Formulation, characterization, antidiabetic, anti-cholinesterase and anti-inflammatory potentials, *Int. J. Pharm.*, 2021, **593**, 120138, DOI: 10.1016/j.ijpharm.2020.120138.

95 A. S. A. Moelyanto, I. Arundina, T. I. Budhy, M. D. C. Surboyo, A. S. Oki and C. H. Ming, Evaluation of Saussurea costus Nanoparticles in the Treatment of Periodontitis: Impact on NF-κB and TNF-α Expression, *Eur. J. Dent.*, 2025, DOI: 10.1055/s-0045-1810069.

96 J. M. Lababidi, M. Fytory, J. El-Qassas, A. T. Gad, O. Mohamed, N. El-Badri and H. M. E.-S. Azzazy, Promising Wound Healing Activity of Saussurea costus Loaded PCL-Gelatin Nanofibers, *Mater. Adv.*, 2025, **6**, 3114–3131, DOI: 10.1039/D4MA01196A.

97 A. J. Alamoudi, S. M. Badr-Eldin, O. A. A. Ahmed, U. A. Fahmy, S. E. I. Elbehairi, M. Y. Alfaifi, H. Z. Asfour, G. A. Mohamed, S. R. M. Ibrahim, A. B. Abdel-Naim, *et al.*, Optimized bilosome-based nanoparticles enhance cytotoxic and pro-apoptotic activity of costunolide in LS174T colon cancer cells, *Biomed. Pharmacother.*, 2023, **168**, 115757, DOI: 10.1016/j.biopha.2023.115757.

98 X. Niu, X. Wang, B. Niu, Y. Meng, H. He, Y. Wang and G. Li, Costunolide Loaded in pH-Responsive Mesoporous Silica Nanoparticles for Increased Stability and an Enhanced Anti-Fibrotic Effect, *Pharmaceuticals*, 2021, **14**(10), 951, DOI: 10.3390/ph14100951.

99 S. Bharathi, B. Ramesh, S. Kumaran, M. Radhakrishnan, D. Saravanan, P. Saravanan, S. R. Pugazhvendan and M. S. Nalinasundari, Development of nanobiomaterial for wound healing based on silver nanoparticles loaded on chitosan hydrogel, *3 Biotech*, 2021, **11**(12), 490, DOI: 10.1007/s13205-021-03030-0.

100 L. A. Kolahalam, K. R. S. Prasad, P. M. Krishna, N. Supraja and S. Shanmugan, The exploration of bio-inspired copper oxide nanoparticles: synthesis, characterization and in-vitro biological investigations, *Heliyon*, 2022, **8**(6), e09726, DOI: 10.1016/j.heliyon.2022.e09726.

101 B. U. Hijazi, M. Faraj, R. Mhanna and M. H. El-Dakdouki, Biosynthesis of silver nanoparticles as a reliable alternative for the catalytic degradation of organic dyes and antibacterial applications, *Curr. Res. Green Sustainable Chem.*, 2024, **8**, 100408, DOI: 10.1016/j.crgsc.2024.100408.

102 M. Riaz, M. Altaf, A. Faisal, M. A. Shekheli, G. A. Miana, M. Q. Khan, M. A. Shah, S. Z. Ilyas and A. A. Khan, Biogenic synthesis of AgNPs with Saussurea lappa CB Clarke and studies on their biochemical properties, *J. Nanosci. Nanotechnol.*, 2018, **18**(12), 8392–8398, DOI: 10.1166/jnn.2018.16414.

103 M. Kumar, D. Kaushik, A. Kumar, H. Krishnan, F. Oz, C. Proestos, A. Hashem and E. F. Abd_Allah, A sustainable approach to prepare green synthesis of copper nanoparticles of *Bauhinia variegata* & *Saussurea lappa*: Unveiling *in vitro* anti-obesity applications, *Heliyon*, 2024, **10**(8), e29433, DOI: 10.1016/j.heliyon.2024.e29433.

104 J. S. Al-Brahim, Saussurea costus extract as bio mediator in synthesis iron oxide nanoparticles (IONPs) and their antimicrobial ability, *PLoS One*, 2023, **18**(3), e0282443, DOI: 10.1371/journal.pone.0282443.

105 B. O. Aljohny, A. A. A. Almaliki, Y. Anwar, M. Ul-Islam and T. Kamal, Antibacterial and Catalytic Performance of Green Synthesized Silver Nanoparticles Embedded in Crosslinked PVA Sheet, *J. Polym. Environ.*, 2021, **29**(10), 3252–3262, DOI: 10.1007/s10924-021-02110-9.

106 A. G. Hussien, W. M. Aboulthana and A. M. Youssef, In vitro evaluation of Saussurea costus gold nano-extract as antioxidant, anti-diabetic, anti-alzheimer, and anti-inflammatory agent, *Egypt. J. Chem.*, 2024, **67**(5), 257–283, DOI: 10.21608/ejchem.2023.244987.8786.

107 L. A. Kolahalam, K. R. S. Prasad, P. Murali Krishna and N. Supraja, Saussurea lappa plant rhizome extract-based zinc oxide nanoparticles: synthesis, characterization and its antibacterial, antifungal activities and cytotoxic studies against Chinese Hamster Ovary (CHO) cell lines, *Heliyon*, 2021, **7**(6), e07265, DOI: 10.1016/j.heliyon.2021.e07265.

108 M. S. S. Adam, A. Taha, M. J. Abdelmageed Abualreish, A. Negm and M. M. Makhlouf, Nanocomposite TiO2/ZnO coated by copper (II) complex of di-Schiff bases with

biological activity evaluation, *Inorg. Chem. Commun.*, 2024, **161**, 112144, DOI: 10.1016/j.inoche.2024.112144.

109 I. Arundina, T. I. Budhy, E. M. Setiawatie, M. D. C. Surboyo, N. Ertanti, C. H. Ming, S. M. Ramaniasari and A. S. A. Moelyanto, Effects of Nanoparticle of Saussurea lappa on Stem Cell from Human Exfoliated Deciduous Teeth (SHED) Proliferation and Cancer Cell Inhibition, *Trop. J. Nat. Prod. Res.*, 2025, **9**(8), 3929–3932, DOI: 10.26538/tjnpr/v9i8.56.

110 N. Zhang, G. Xiong and Z. Liu, Toxicity of metal-based nanoparticles: Challenges in the nano era, *Front. Bioeng. Biotechnol.*, 2022, **10**, 1001572, DOI: 10.3389/fbioe.2022.1001572.

111 Y. Min, G. G. D. Suminda, Y. Heo, M. Kim, M. Ghosh and Y.-O. Son, Metal-Based Nanoparticles and Their Relevant Consequences on Cytotoxicity Cascade and Induced Oxidative Stress, *Antioxidants*, 2023, **12**(3), 703, DOI: 10.3390/antiox12030703.

112 Z. Ferdous and A. Nemmar, Health Impact of Silver Nanoparticles: A Review of the Biodistribution and Toxicity Following Various Routes of Exposure, *Int. J. Mol. Sci.*, 2020, **21**(7), 2375, DOI: 10.3390/ijms21072375.

113 Z. Goktas, Y. Zu, M. Abbasi, S. Galyean, D. Wu, Z. Fan and S. Wang, Recent advances in nanoencapsulation of phytochemicals to combat obesity and its comorbidities, *J. Agric. Food Chem.*, 2020, **68**(31), 8119–8131, DOI: 10.1021/acs.jafc.0c00131.

114 P. Xiong, X. Huang, N. Ye, Q. Lu, G. Zhang, S. Peng, H. Wang and Y. Liu, Cytotoxicity of metal-based nanoparticles: from mechanisms and methods of evaluation to pathological manifestations, *Adv. Sci.*, 2022, **9**(16), 2106049, DOI: 10.1002/advs.202106049.